Ultrafast photooxidation of protein-bound anionic flavin radicals

Bo Zhuang, Rivo Ramodiharilafy, Ursula Liebl, Alexey Aleksandrov, Marten H. Vos

PNAS
www.pnas.org

Main Manuscript for

Ultrafast Photooxidation of Protein-Bound Anionic Flavin Radicals

Bo Zhuang, Rivo Ramodiharilafy, Ursula Liebl, Alexey Aleksandrov*, and Marten H. Vos*

LOB, CNRS, INSERM, École Polytechnique, Institut Polytechnique de Paris, 91128 Palaiseau, France

*Alexey Aleksandrov

Email: alexey.aleksandrov@polytechnique.edu

*Marten H. Vos

Email: marten.vos@polytechnique.edu

Author Contributions: B.Z. and M.H.V. designed research; B.Z., R.R., A.A. and M.H.V. performed research; B.Z. and A.A. designed new reagants/analytical tools; B.H.Z and A.A. analyzed data; B.Z., U.L.., A.A. and M.H.V. provided critical feedback on the results and manuscript; and B.Z., U.L.., A.A. and M.H.V. wrote the paper.

Competing Interest Statement: The authors declare no competing financial interest.

Classification: Biological Sciences/Biophysics and Computational Biology; Physical Sciences/Chemistry

Keywords: Electron transfer, Flavoproteins, Ultrafast Spectroscopy, Molecular modeling

This PDF file includes:

Main Text
Figures 1 to 5

Abstract

The photophysical properties of anionic semi-reduced flavin radicals are essentially unknown despite their importance in numerous biochemical reactions. Here, we studied the photoproducts of these intrinsically unstable species in five different flavoprotein oxidases where they can be stabilized, including the well-characterized glucose oxidase. Using ultrafast absorption and fluorescence spectroscopy, we unexpectedly found that photoexcitation systematically results in the oxidation of protein-bound anionic flavin radicals on a time scale less than ~100 fs. The thus generated photoproducts decay back in the remarkably narrow 10–20 ps time range. Based on molecular dynamics and quantum mechanics computations, positively charged active-site histidine and arginine residues are proposed to be the electron acceptor candidates. Altogether we established that, in addition to the commonly known and extensively studied photoreduction of oxidized flavins in flavoproteins, the reverse process, i.e., the photooxidation of anionic flavin radicals, can also occur. We propose that this process may constitute a universal excited-state deactivation pathway for protein-bound anionic flavin radicals. Our findings reveal a novel photochemical reaction in flavoproteins and further extend the family of flavin photocycles.

Significance Statement

Flavoproteins are colored proteins involved in a large variety of biochemical reactions. They can perform photochemical reactions, which are increasingly exploited for bioengineering new protein-derived photocatalysts. In particular, light-induced reduction of the resting oxidized state of the flavin by close-lying amino acids or substrates, is extensively studied. Here, we demonstrate that the reverse and previously unknown reaction, photooxidation of the semi-reduced flavin radical, a short-lived reaction intermediate in many biochemical reactions, efficiently occurs in flavoprotein oxidases. We anticipate that this finding will allow photoreduction of external reactants and lead to exploration of novel photocatalytic pathways.

Main Text

Introduction

Flavoproteins are ubiquitous components in key biological processes, in particular involved in redox reactions critical to the major metabolic energy transformations and electron transfer (ET) chains (1–3). The flavin cofactor usually exists as riboflavin (RFl), i.e., vitamin B_2, derivative flavin mononucleotide (FMN) or, more often, flavin adenine dinucleotide (FAD). Flavin groups are versatile redox partners as they can adopt three different redox states, each with different possible protonation states, overall including five physiologically relevant chemical forms (Fig. 1A) (4).

Flavins are colored molecules and photochemical processes are known to occur in many flavoproteins; in some specific cases these processes play a functional role. Photoinduced phenomena of oxidized flavin, the resting state in most flavoproteins, have been studied extensively. Oxidized flavin is strongly fluorescent in solution, but when bound to proteins its fluorescence is often quenched as it may act as electron acceptor and participate in photoinduced ET reactions (5–11). Fully reduced (neutral, or anionic) flavins emit weak fluorescence in solution, but in a confined protein environment, or at low temperature, their fluorescence is greatly enhanced, a phenomenon ascribed to hindering of deactivation by bending motions of the isoalloxazine ring (12, 13). Semi-reduced (neutral, or anionic) flavin radicals are usually short-lived species formed in the catalytic cycles of flavoproteins, and in solution cannot be obtained as free radicals in the steady state. In some flavoproteins where neutral flavin radicals can be stabilized, e.g., DNA photolyase and flavodoxin, excitation has been reported to extract an electron from nearby aromatic residues (12, 14–16); in DNA photolyase this process generates the long-lived and catalytically

active, fully reduced flavin cofactor (17). In contrast, how anionic flavin radicals behave upon excitation remains unclear, despite their relevance as functional intermediates in many flavoproteins.

In blue-light receptor proteins such as cryptochromes and BLUF domain proteins, the photoreduction of oxidized flavin (FMN_{ox}, or FAD_{ox}) to the anionic radical form ($FMN^{\bullet-}$, or $FAD^{\bullet-}$) represents the first essential step in their response to light (18, 19). In fatty acid photodecarboxylase, the photoinduced ET between FAD_{ox} and the fatty acid substrate leads to $FAD^{\bullet-}$ as an intermediate (20). The catalytic activity of the flavoprotein monooxygenase PqsL can be triggered by blue-light illumination, which was proposed to occur via photoinduced formation of the $NAD(P)H^{\bullet+}/FAD^{\bullet-}$ radical pair (21). Light-independent processes can also occur through pathways involving anionic flavin radical formation. This is for instance the case for the oxidative catalysis of organic molecules by nitronate monooxygenase (NMO) (22) and by glucose oxidase (GOX), which is widely used in biotechnology applications (23, 24). Yet, despite decennia of in-depth flavoprotein research, so far only a few flavoproteins have been reported to be able to stabilize the anionic flavin radical in the steady state (18, 25–30). As a result, understanding of their photophysical properties is limited.

In general, radical ions in open-shell configurations have distinct photophysical properties from those of their closed-shell parent molecules. Their excited states usually decay in a complex manner, involving efficient internal conversion, or conical intersections between excited state and ground state (31, 32); with electron donors or acceptors close-by, ultrafast ET can also take place (33, 34). The present work provides the first ultrafast spectroscopic investigation with full spectral resolution to elucidate the actual deactivation pathway of protein-bound anionic flavin radicals. In particular, we studied a set of different flavoprotein oxidases, where the anionic flavin radicals can be stabilized and of which well-characterized crystal structures are available, i.e., $FAD^{\bullet-}$ in GOX, choline oxidase (COX), monomeric sarcosine oxidase (MSOX) and D-amino acid oxidase (DAAO), as well as $FMN^{\bullet-}$ in NMO. In all these enzymes, the active site contains positively charged residues that are thought to be required for stabilizing the superoxide $O_2^{\bullet-}$ functional reaction intermediate ("oxygen activation") (35, 36). In all systems, these include residues that are close to van der Waals contact with the isoalloxazine ring system (Fig. 1B).

In photoinduced ET processes, flavin species almost always act as electron acceptors and are photo-reduced, as is the case with protein-bound oxidized flavins and neutral flavin radicals (8, 10, 11, 15, 16). The only known exception in nature thus far is DNA photolyase. In the photo-repair process of both CPD and (6–4) photolyases, the flavin cofactors function in the fully reduced, anionic form $FADH^-$, the repair of UV-induced DNA lesions is initiated by photoinduced ET from $FADH^-$ to the DNA substrate, yielding the neutral flavin radical ($FADH^{\bullet}$) (17, 37). Recently, a similar photoreaction in flavin-dependent "ene"-reductases has been exploited as a tool to initialize stereoselective radical cyclization reactions in organic synthesis (38). Our present findings reveal yet another reaction pathway in the photochemistry of flavoproteins, namely, the ultrafast photooxidation of anionic flavin radicals. We establish that excitation of these species results in their photooxidation on a time scale less than ~100 fs, generating oxidized flavins in the transient product state that decay in 10–20 ps back to the anionic radical forms. As similar phenomena were observed for all five flavoprotein oxidases in our study, such a photooxidation reaction might constitute an intrinsic characteristic of protein-bound anionic flavin radicals in general. We further discuss the identity of potential electron acceptors based on density-functional theory (DFT) calculations and molecular dynamics (MD) simulations, as well as hybrid quantum mechanics/molecular mechanics (QM/MM) methods.

Results

Steady-state absorption spectra of anionic flavin radicals.

Anionic flavin radicals are usually short-lived reaction intermediates, and in solution their formation and detection requires pulse radiolysis methods (39). In some flavoproteins anionic flavin radicals can be produced and stabilized under anaerobic conditions by blue-light illumination in the

presence of a hole scavenger, or through chemical reduction. Fig 1C shows the absorption spectra of protein-bound anionic flavin radicals produced and stabilized in GOX, COX, MSOX, DAAO and NMO. In the visible range, anionic flavin radicals exhibit two distinct transition bands (assigned to $D_0 \rightarrow D_4$ and $D_0 \rightarrow D_6$ transitions) (10). Those obtained in proteins differ significantly from those produced in solution by pulse radiolysis and from each other. This can be explained by the interactions between the anionic flavin radicals and the local protein environments, and might be an indication of positive charges close-by, as has been demonstrated in our previous work (10). A QM/MM calculation (Fig 1D) shows that the protein environment of GOX significantly lowers the highest occupied molecular orbital (HOMO) and lowest unoccupied molecular orbital (LUMO) energy levels of $FAD^{\bullet-}$ compared with those in vacuum, indicating the effects of the protein environment on the electronic properties of $FAD^{\bullet-}$. Furthermore, we note that the presence of small amounts of oxidized or fully reduced flavin in the equilibrated samples cannot be fully excluded (see *SI Note 1*).

Emission from excited anionic flavin radicals.

First, we investigated the excited state dynamics of $FAD^{\bullet-}$ using time-resolved fluorescence measurements. As shown in Fig. 2A and Fig. S5, upon excitation at 390 nm we did not detect any perceptible emission signal for $FAD^{\bullet-}$ in GOX with our setup that has femtosecond time-resolution (for samples obtained either by photo- or chemical reduction). The fluorescence decays of FAD_{ox} and $FADH^-$ in GOX measured under the same experimental conditions are presented in the same figure for comparison. The fluorescence of FAD_{ox} in GOX mainly decays with time-constants of 1.1 ps and 4.3 ps (5, 11). The time-resolved fluorescence of $FADH^-$ in GOX exhibits monophasic decay with a time constant of 800 ps (Fig. S6b and Table S2). The absence of an emission signal for $FAD^{\bullet-}$ in GOX indicates that there are nonradiative processes taking place much faster than the instrument response (~ 200 fs with suprasil as Kerr medium).

$FAD^{\bullet-}$ in COX is stable even in the presence of O_2 (30), allowing long-duration signal accumulation for detecting small signals. As a reference, the time-resolved fluorescence of non-reduced, FAD_{ox}-containing (Fig. S1) COX was measured (Fig. 2B) and is reported here for the first time. Upon excitation at 390 nm, it exhibits a biphasic decay with a dominant ~300-fs ultrafast phase and a long-lived phase (Fig. S7a). The 300-fs phase was assigned to FAD_{ox} fluorescence, quenched by flavin photoreduction processes, with Tyr465 and Trp61 being the potential quenchers (Fig. S10). The sample was then incubated with $Na_2S_2O_4$ until the reaction reached maximal $FAD^{\bullet-}$ formation (corresponding to the absorption spectrum shown in Fig. 1C), and further time-resolved fluorescence measurements were performed. With benzene as Kerr medium (relatively high sensitivity, but low time-resolution), a small signal less than 10% of that of FAD_{ox} was detected. It has similar kinetic and spectral (maximum at ~520 nm) features (Fig. 2B and Fig. S7) to those of FAD_{ox}, and was therefore assigned to a remaining fraction of FAD_{ox}. On the other hand, when suprasil was used as Kerr medium (low sensitivity, but high time-resolution), no perceptible emission signal was detected for the reduced sample, whereas the ~300 fs phase of FAD_{ox} is clearly resolved in the non-reduced sample (inset, Fig. 2B). From the comparison of the signals of the reduced and non-reduced samples we estimate that any $FAD^{\bullet-}$ fluorescence decays in < 30 fs. Altogether, we conclude that as in GOX, in COX ultrafast nonradiative deactivation of excited-state $FAD^{\bullet-}$ occurs.

Transient formation of oxidized flavins upon the excitation of anionic flavin radicals.

The lack of emission in radical ions is usually explained by efficient internal conversion between D_1 and D_0 states, involvement of D_2/D_1 and D_1/D_0 conical intersections, or photoinduced ET when there is an electron donor or acceptor close-by (31–34). To investigate the actual excited-state deactivation pathways of protein-bound anionic flavin radicals, we performed transient absorption measurements. Pump pulses centered at 390 and 520 nm were used to excite the two distinct transition bands.

The transient absorption kinetics of $FAD^{\bullet-}$ in GOX are shown in Fig. 3A, and the decay associated spectra (DAS) extracted from the global analysis are given in Fig. 3B and Fig. S13. Upon excitation, we observed a marked induced absorption band formed within ~100 fs. This band

is very similar to the $S_0 \rightarrow S_1$ transition band of ground state FAD_{ox}. Under 520-nm excitation the decay of this band (time constant 19 ps) constitutes the only spectral evolution. Under 390 nm excitation this band has virtually identical shape (Fig. 3B) and decays with a very similar time constant. Along with the fact that we did not observe any emission with a similar lifetime in the time-resolved fluorescence measurements (*vide supra*), we conclude that this ~20 ps phase must arise from a non-emissive product state.

The 390-nm excitation data require two additional small kinetic phases with time constants of 1.8 and 900 ps to obtain a satisfactory global fit (Fig. 3A and Fig. S13). These time constants are similar to those of the excited-state lifetime of FAD_{ox} and $FADH^-$ (1.1/4.3 ps and 800 ps, respectively, *vide supra*) in GOX; the corresponding DAS, although too small to be reliably analyzed, also show resemblance to those obtained for FAD_{ox} (11) and $FADH^-$ (Fig. S11, S12) (13). Indeed, as illustrated in Fig. 1C, the 390-nm pump will also excite trace amounts of oxidized and fully reduced flavins, whereas the 520-nm pump can only excite anionic flavin radicals.

In Fig. 3, B and D, spectral analysis is performed by comparing the DAS of the product states with steady-state difference spectra of the oxidized flavin and the anionic flavin radical. The overall features of the DAS, including the ground state bleaching and induced absorption, correspond well with the model spectra. Furthermore, taking into account the excitation density using $[Ru(bpy)_3]Cl_2$ as a reference, the amplitude of the signals indicates near-unity oxidized flavin formation per absorbed photon (see *SI Note 4* for details).

Yet, the DAS are not strictly identical to the model spectra. This may be due to two reasons. First, given the ultrafast time scale, the transiently formed oxidized flavins are presumably in an unrelaxed protein environment resulting in a shifted absorption spectrum and altered vibrational progression. Second, during the photooxidation process, a radical intermediate formed from a yet unknown electron acceptor may also absorb in the visible region and contribute to the observed DAS. The second assumption is supported by the analysis of the transient anisotropy absorption spectra (Fig. S18), which provides detailed insight in the orientation of the involved transition dipole moments (40). (Details for calculating anisotropy r and the angle ϕ between the pumped and probed transition are given in *SI Note 5*) In the 440–470 nm spectral range where the transient absorption is maximal, the anisotropies are almost constant and very similar for 390-nm (r = 0.18–0.19) and 520-nm (r = 0.20–0.22) excitation. As in both cases mainly the $S_0 \rightarrow S_1$ transition band of FAD_{ox} was probed, this result indicates that the $D_0 \rightarrow D_4$ and $D_0 \rightarrow D_6$ transition dipole moments of $FAD^{\bullet-}$ in GOX are near-parallel, which is in general agreement with the theoretical prediction that these two transition dipole moments form a small angle (Fig. S19). However, previous work has shown that the $S_0 \rightarrow S_1$ transition dipole moment of FAD_{ox} should also be near-parallel to the $D_0 \rightarrow D_4$ transition of $FAD^{\bullet-}$, which corresponds to a r value close to 0.4 (9), whereas smaller values were observed in the present case. This may be explained by broad contributions from transition dipole moments of a third species in the probed region. The identity of this third species is examined in the next section.

Additionally, we investigated whether the photoinduced flavin oxidation depends on the preparation method of $FAD^{\bullet-}$ or on the pH in GOX. No such dependence was observed (Fig. S16) and this robustness, along with our observations in a multitude of protein systems, strongly suggests that photooxidation of the anionic flavin radical occurs ubiquitously in flavoenzymes where this species can be formed.

Identity of the electron acceptor.

With regard to the possible identity of the corresponding electron acceptors, we rule out the involvement of by-products produced upon preparing the anionic flavin radicals in the steady state, as similar results were obtained with different reduction methods, including photoreduction. The ultrafast formation of the transient oxidized flavins and the monophasic decays suggested a close interaction and a well-defined conformation between the electron donor and acceptor, which makes active-site residues appropriate candidates.

In DFT, the ionization potential (IP) and the electron affinity (EA) of a molecule can be approximated by the negative of the HOMO energy, which to be more precise refers to the highest occupied Kohn–Sham (KS) levels here, of the N and $N + 1$ electron systems, respectively (41). For

selected active-site residues in the investigated flavoprotein oxidases, DFT calculations were thus carried out to evaluate their EA by optimizing their geometries in the one-electron-reduced forms (*N + 1*). The result shows that in vacuum only the neutral radicals of fully protonated histidine and arginine have reasonable negative HOMO energies (−5.24 and −5.92 eV, respectively), indicating the relatively high (and close) EA, whereas for the other residues, including the singly protonated forms of histidine, the acceptance of an additional electron leads to relatively unstable species (Table S4). Indeed, among the one-electron-reduced forms of common amino acids, so far only the neutral radicals of isolated protonated histidine and arginine (or analogues) have been experimentally produced and spectrally characterized (42, 43). Together, this suggests that fully protonated histidine and arginine are the most likely candidates for the electron acceptors among those residues. Notably, the neutral lysine radical appears to have a moderately negative HOMO energy (−3.77 eV). Therefore, protonated lysine is energetically less favorable to act as electron acceptor compared with fully protonated histidine and arginine.

Among the five flavoprotein oxidases, the structural properties of GOX are the most extensively studied and relatively well-understood, making it an appropriate system for further theoretical investigation of the electron acceptor. In GOX, there are two histidine residues located very close to the flavin in the active site (Fig. 1B), i.e., His516 and His559 (3.83 Å and 3.76 Å ring-ring distance to FAD in the crystal structure, respectively). In accord with the DFT calculations above, a doubly protonated form of histidine is more likely to act as electron acceptor; therefore we examined the protonation state of these two histidines. His559 forms strong hydrogen bonds to Glu412 and is expected to be double protonated over a wide pH range (44, 45). On the other hand, the protonation state of His516 in the presence of $FAD^{\bullet-}$ is less clear, which was examined molecular dynamics free energy (MDFE) simulations. The result (Table S5) shows that, in the presence of $FAD^{\bullet-}$, His516 also has a very high pK_a of 13.5 (SD: 0.7), due to interactions with the negatively charged $FAD^{\bullet-}$ and nearby Asp328. Therefore, in GOX both histidine residues, His516 and His559, are likely to be doubly protonated in the presence of $FAD^{\bullet-}$. The active site of GOX appears to be arranged in a way that in the reduced form the pK_a of the flavin cofactor is downshifted (46), while the pK_a values of the two histidines are upshifted.

MD simulations were then performed for GOX with the flavin in the anionic radical state and both His516 and His559 doubly protonated. As shown in Fig. 4A, throughout the 150-ns MD simulation, His559 remains very close to $FAD^{\bullet-}$ with an average minimal ring-to-ring distance of 3.81 Å. On the other hand, His516 rotates around χ2 to a noncatalytic conformation, as it was shown previously (47), and stays relatively far away from $FAD^{\bullet-}$ (~5.5 Å), and only transiently approaches the cofactor. The shorter distance of 3.83 Å between flavin and His516 observed in the crystal structure is explained by the fact that His516 is singly protonated with FAD_{ox} in the crystal structure (44, 47). The finding of His516 conformational changes is in agreement with a previous study showing that His516 is a flexible, functionally important residue that can flip between catalytic and noncatalytic conformations (47). Given the closer interactions of His559 with $FAD^{\bullet-}$, His559 appears to be a suitable candidate for accepting an electron from excited $FAD^{\bullet-}$. These results were also reproduced well by the simulations based on a different high-resolution crystal structure (Fig. S20; PDB entry: 3QVP, resolution: 1.2 Å).

Assuming His559 as the electron acceptor, we employed a QM/MM protocol to calculate the transient absorption spectra of $FAD^{\bullet-}$ photooxidation in GOX, including the induced absorption of FAD_{ox} and $HisH_2^{\bullet}$, as well as the ground-state bleaching of $FAD^{\bullet-}$ ($HisH_2^+$ only absorbs in the ultraviolet range). As shown in Fig. 4, B and C, despite some overestimations of the transition energies, the calculated spectra of FAD_{ox} and $FAD^{\bullet-}$ agree well with the experimental spectra (Fig. 1C). In the near ultraviolet range, the calculated spectrum of $HisH_2^{\bullet}$ in aqueous solution agrees well with the experimental spectrum obtained by pulse radiolysis (42, 48). Notably, in GOX, $HisH_2^{\bullet}$ formed from His559 displays more intense absorption in the visible/near-infrared range compared with its state in solution (inset of Fig. 4B), presumably due to effects of the complex protein environment around His559, in particular the hydrogen-bonded Glu412. This partially compensates

the bleaching of $FAD^{\bullet-}$ and leads to a red-extending tail in the overall difference spectrum, which reproduces the experimental DAS reasonably well (Fig. 4D).

The free energy change associated with the $FAD^{\bullet-}/HisH_2^+ \rightarrow FAD_{ox}/HisH_2^{\bullet}$ ET reaction in GOX was estimated using the following method. In a protein system, the free energy change of the investigated ET process ($\Delta G_{ET,prot}$) can be calculated by evaluating the electrostatic free energy difference of the two states relative to a reference system in the aqueous solvent:

$$\Delta G_{ET,prot} = \Delta G_{ET,solv} + \Delta\Delta G_{ES}$$

where $\Delta G_{ET,solv}$ is the free energy change of the investigated ET process in the aqueous solution obtained by high-level QM calculations (49, 50); $\Delta\Delta G_{ES}$ is the double difference of electrostatic energies of the systems before ($FAD^{\bullet-}/HisH_2^+$) and after ($FAD_{ox}/HisH_2^{\bullet}$) the ET reaction, respectively, evaluated using MD simulations and the Poisson-Boltzmann (PB) method (51) (see *SI Note 7* for further details) in the protein relative to the aqueous solvent. Based on this approach, we obtained a $\Delta G_{ET,prot}$ value of 2.19 (SD: 0.05) eV, which is less than the energy of a 520-nm photon (2.38 eV, corresponding to the red edge of the $FAD^{\bullet-}$ absorption), confirming that such a *photoinduced* ET reaction is energetically feasible. It is also worth noting that the protein environment is found to disfavor the ET reaction $\Delta\Delta G_{ES}$ = +0.23 (SD: 0.05) eV), hinting at the stabilization of the charges of $FAD^{\bullet-}$ and $His559^+$ by surrounding residues in the active site of GOX.

Discussion

Taken together, our time-resolved fluorescence and transient absorption measurements provide a consistent, yet unexpected, picture that ultrafast photooxidation of anionic flavin radicals occurs in GOX, COX, MSOX, DAAO and NMO. In all systems this process is followed by back transfer of the ejected electron on the picosecond timescale, as evidenced from the monophasic decay of the induced absorption band (Fig. 3C) and the absence of bleaching signals of the anionic flavin radical on longer timescales (Fig. 3A). The very similar observations among the five different oxidases indicate that the ET reactions involve similar distances and electronic properties. As illustrated in Fig. 1B and summarized in Table S3, in the five flavoprotein oxidases investigated in this study (and possibly for all other functional flavoprotein oxidases), there is always a positively charged residue, including either histidine or arginine, present in the active site (22, 35, 52, 53). Our present results suggest that these residues not only play an important role in the thermodynamic stabilization of anionic flavin radicals (36), but also contribute to the deactivation of the excited-state anionic flavin radicals via a charge-transfer state. As the presence of close-lying positively charged residues can be considered a prerequisite for the formation and stabilization of anionic flavin radicals in proteins, the photooxidation process may constitute a universal excited-state deactivation pathway for protein-bound anionic flavin radicals. Qualitatively, such properties may also be related to the common requirements of these oxidases to stabilize the electron-rich intermediates in their catalytic cycles (35), including the highly reactive reaction intermediate $O2^{\bullet-}$ in the active site, by a positive charge in close proximity to the flavin (36, 45).

In none of the investigated systems we have been able to detect fluorescence assignable to the anionic flavin radicals, in agreement with the extremely rapid appearance of the oxidized flavin photoproduct. For COX, our assessment of lack of time-resolved $FAD^{\bullet-}$ fluorescence contrasts with the report of $FAD^{\bullet-}$-assigned steady-state fluorescence peaking around 450 nm (at the blue of the 500 nm $FAD^{\bullet-}$ absorption maximum, i.e., violating the Kasha–Vavilov rule) in the enzyme from *A. globiformis* (30). We note that C4a-flavin adducts, which can form in COX (54), strongly fluoresce in this region (55, 56). The only time-resolved fluorescence assigned to the anionic flavin radical remains that from insect cryptochrome (12, 27). Yet, the spectral characteristics are very close to those of oxidized flavin, as discussed in Ref. (26). Indeed, the reported absorption spectrum of $FAD^{\bullet-}$ in this protein (27) is significantly different from another report of $FAD^{\bullet-}$ in *Drosophila* cryptochrome (18) in that it shows an unusual plateau at ~450 nm,, near the absorption maximum of FAD_{ox} (Fig. S4).

The lifetimes of the formed photoproducts in the flavoprotein oxidases studied span a remarkably narrow range of ~10–20 ps, with three of the lifetimes being at 20 ps within experimental error. This finding may be linked to the very similar and close distances between the flavins and nearby histidine or arginine residues in the five flavoprotein oxidases (Fig. 1B), as well as the similar EA of histidine and arginine residues (Table S4). In this context we note that in COX the covalently linked and functionally relevant histidine, His99 (57), is most probably neutral, since in the crystal structure its N_δ atom does not appear to have any hydrogen bond partners, and the pK_a of 8α-*N*-imidazole-substituted flavins is determined to be ~6 (N of the imidazole moiety) in solution (58). Therefore, it is not a likely electron acceptor, making His466 a more probable candidate.

It is of note that the crystal structures of the proteins studied *a priori* correspond to those with oxidized flavins, and additionally for COX to a protein variant and for DAAO to a protein–inhibitor complex. When the flavins are reduced, the active-site conformations are likely to contain rearrangements, as shown above for GOX. This makes quantitative evaluation of ET dynamics and a definitive determination of the electron acceptor(s) challenging at this point. Moreover, variants of the close-lying positively charged residues are likely to influence the formation and stabilization of anionic flavin radicals, as well as affect the binding affinity for flavins (45, 53, 59). Future studies combining more extensive theoretical investigations and spectroscopic experiments on genetically modified proteins will allow determining the exact nature of the electron acceptors and ultimately establish the precise molecular origin of the common dynamic features of ET in flavoprotein oxidases.

In summary, in this work we have demonstrated a novel photochemical reaction occurring in the anionic radical state of flavoprotein oxidases, further extending the variety of light-induced processes in this important class of enzymes (Fig. 5). In view of the ephemeral nature of anionic flavin radicals in most biochemical and photobiochemical reactions where it could act as an intermediate, whether the here-characterized photoreaction could play a physiological or photoprotective role in native proteins remains to be established. By genetic engineering approaches we envisage to explore the possibilities of creating pathways that allow further electron hopping, thus stabilizing the primary photoproduct. These approaches *in fine* will allow photoreduction of external reactants and pave the way towards the development of a novel class of flavoprotein photocatalysts.

Materials and Methods

GOX from *Aspergillus niger*, COX from *Arthrobacter sp.*, MSOX from *Bacillus sp.* and DAAO from porcine kidney were purchased from Sigma-Aldrich. NMO from *Pseudomonas aeruginosa* was expressed using a codon-optimized expression vector and purified following standard procedures. The anionic flavin radicals in these oxidases were prepared by previously reported methods with slight modifications (25, 26, 60).

The setup for time-resolved fluorescence employs a Kerr gate (61), and multicolor time-resolved absorption spectra were recorded by the pump–probe technique (9, 10), based on an instrument operating at 500 Hz. Global analysis of the data was performed using the Glotaran program (62).

DFT calculations were carried out using the ORCA program (version: 4.2) (63) to optimize the geometries and estimate the energies of studied molecules. For GOX, MDFE simulations for calculating pK_a values and full-protein MD simulations were carried out using the NAMD programs (version 2.13) (64). Hybrid QM/MM calculations were carried out using the pDynamo program (version 1.9.0) (65) coupled with the ORCA package to obtain the KS levels, and further estimate the spectral properties of studied molecules based on time-dependent DFT (TDDFT). The PB equation was solved using the CHARMM program (version: 45b2) (66) to evaluate electrostatic energies in the protein and solution for computing free energy changes of redox processes.

A detailed description of the experimental procedures, data analysis, and simulation protocols is given in *SI Methods*.

Acknowledgments

B.Z. thanks the China Scholarship Council for providing a Ph.D. scholarship.

References

1. C. Walsh, Flavin Coenzymes: At the crossroads of biological redox chemistry. *Acc. Chem. Res.* **13**, 148–155 (1980).
2. M. W. Fraaije, A. Mattevi, Flavoenzymes: diverse catalysts with recurrent features. *Trends Biochem. Sci.* **25**, 126–132 (2000).
3. W. P. Dijkman, G. De Gonzalo, A. Mattevi, M. W. Fraaije, Flavoprotein oxidases: classification and applications. *Appl. Microbiol. Biotechnol.* **97**, 5177–5188 (2013).
4. R. Miura, Versatility and specificity in flavoenzymes: Control mechanisms of flavin reactivity. *Chem. Rec.* **1**, 183–194 (2001).
5. D. Zhong, A. H. Zewail, Femtosecond dynamics of flavoproteins: charge separation and recombination in riboflavine (vitamin B2)-binding protein and in glucose oxidase enzyme. *Proc. Natl. Acad. Sci. U. S. A.* **98**, 11867–11872 (2001).
6. N. Nunthaboot, *et al.*, Simultaneous analysis of ultrafast fluorescence decays of FMN binding protein and its mutated proteins by molecular dynamic simulation and electron transfer theory. *J. Phys. Chem. B* **112**, 13121–13127 (2008).
7. S. P. Laptenok, *et al.*, Ultrafast real-time visualization of active site flexibility of flavoenzyme thymidylate synthase ThyX. *Proc. Natl. Acad. Sci. U. S. A.* **110**, 8924–8929 (2013).
8. F. Lacombat, *et al.*, Ultrafast oxidation of a tyrosine by proton-coupled electron transfer promotes light activation of an animal-like cryptochrome. *J. Am. Chem. Soc.* **141**, 13394–13409 (2019).
9. L. Nag, P. Sournia, H. Myllykallio, U. Liebl, M. H. Vos, Identification of the TyrOH•+ radical cation in the flavoenzyme TrmFO. *J. Am. Chem. Soc.* **139**, 11500–11505 (2017).
10. B. Zhuang, D. Seo, A. Aleksandrov, M. H. Vos, Characterization of light-induced, short-lived interacting radicals in the active site of flavoprotein ferredoxin-NADP+ oxidoreductase. *J. Am. Chem. Soc.* **143**, 2757–2768 (2021).
11. L. Nag, A. Lukacs, M. H. Vos, Short-lived radical intermediates in the photochemistry of glucose oxidase. *ChemPhysChem* **20**, 1793–1798 (2019).
12. Y. T. Kao, *et al.*, Ultrafast dynamics of flavins in five redox states. *J. Am. Chem. Soc.* **130**, 13132–13139 (2008).
13. M. Enescu, L. Lindqvist, B. Soep, Excited-state dynamics of fully reduced flavins and flavoenzymes studied at subpicosecond time resolution. *Photochem. Photobiol.* **68**, 150–156 (1998).
14. J. Pan, *et al.*, Excited-state properties of flavin radicals in flavoproteins: femtosecond spectroscopy of DNA photolyase, glucose oxidase, and flavodoxin. *J. Phys. Chem. B* ***108***, 10160–10167 (2004).
15. M. Kundu, T. F. He, Y. Lu, L. Wang, D. Zhong, Short-range electron transfer in reduced flavodoxin: ultrafast nonequilibrium dynamics coupled with protein fluctuations. *J. Phys. Chem. Lett.* **9**, 2782–2790 (2018).
16. A. Lukacs, A. P. M. Eker, M. Byrdin, K. Brettel, M. H. Vos, Electron hopping through the 15 Å triple tryptophan molecular wire in DNA photolyase occurs within 30 ps. *J. Am. Chem. Soc.* **130**, 14394–14395 (2008).
17. K. Brettel, M. Byrdin, Reaction mechanisms of DNA photolyase. *Curr. Opin. Struct. Biol.* **20**, 693–701 (2010).
18. A. Berndt, *et al.*, A novel photoreaction mechanism for the circadian blue light photoreceptor Drosophila cryptochrome. *J. Biol. Chem.* **282**, 13011–13021 (2007).
19. M. Gauden, *et al.*, Hydrogen-bond switching through a radical pair mechanism in a flavin-binding photoreceptor. *Proc. Natl. Acad. Sci. U. S. A.* **103**, 10895–10900 (2006).

20. D. Sorigué, *et al.*, Mechanism and dynamics of fatty acid photodecarboxylase. *Science* **372**, eabd5687 (2021).
21. S. Ernst, S. Rovida, A. Mattevi, S. Fetzner, S. L. Drees, Photoinduced monooxygenation involving NAD(P)H-FAD sequential single-electron transfer. *Nat. Commun.* **11**, 1–11 (2020).
22. G. Gadda, K. Francis, Nitronate monooxygenase, a model for anionic flavin semiquinone intermediates in oxidative catalysis. *Arch. Biochem. Biophys.* **493**, 53–61 (2010).
23. D. J. T. Porters, H. J. Bright, Mechanism of oxidation of nitroethane by glucose oxidase. *J. Biol. Chem.* **252**, 4361–4370 (1977).
24. S. B. Bankar, M. V. Bule, R. S. Singhal, L. Ananthanarayan, Glucose oxidase - an overview. *Biotechnol. Adv.* **27**, 489–501 (2009).
25. V. Massey, G. Palmer, On the existence of spectrally distinct classes of flavoprotein semiquinones. A new method for the quantitative production of flavoprotein semiquinones. *Biochemistry* **5**, 3181–3189 (1966).
26. D. Su, *et al.*, Fluorescence properties of flavin semiquinone radicals in nitronate monooxygenase. *ChemBioChem* **20**, 1646–1652 (2019).
27. Y.-T. Kao, *et al.*, Ultrafast dynamics and anionic active states of the flavin cofactor in cryptochrome and photolyase. *J. Am. Chem. Soc*. **130**, 7695–7701 (2008).
28. M. Medina, A. Vrielink, R. Cammack, ESR and electron nuclear double resonance characterization of the cholesterol oxidase from Brevibacterium sterolicum in its semiquinone state. *Eur. J. Biochem.* **222**, 941–947 (1994).
29. M. A. Wagner, P. Trickey, Z. W. Che, F. S. Mathews, M. S. Jorns, Monomeric sarcosine oxidase: 1. flavin reactivity and active site binding determinants. *Biochemistry* **39**, 8813–8824 (2000).
30. M. Ghanem, F. Fan, K. Francis, G. Gadda, Spectroscopic and kinetic properties of recombinant choline oxidase from Arthrobacter globiformis. *Biochemistry* **42**, 15179–15188 (2003).
31. J. Grilj, E. N. Laricheva, M. Olivucci, E. Vauthey, Fluorescence of radical ions in liquid solution: Wurster's blue as a case study. *Angew. Chemie - Int. Ed.* **50**, 4496–4498 (2011).
32. D. T. Breslin, M. A. Fox, Excited-state behavior of thermally stable radical ions. *J. Phys. Chem.* **98**, 408–411 (1994).
33. M. Fujitsuka, S. S. Kim, C. Lu, S. Tojo, T. Majima, Intermolecular and intramolecular electron transfer processes from excited naphthalene diimide radical anions. *J. Phys. Chem. B* **119**, 7275–7282 (2015).
34. J. A. Christensen, *et al.*, Phenothiazine radical cation excited states as super-oxidants for energy-demanding reactions. *J. Am. Chem. Soc.* **140**, 5290–5299 (2018).
35. M. Ghanem, G. Gadda, Effects of reversing the protein positive charge in the proximity of the flavin N(1) locus of choline oxidase. *Biochemistry* **45**, 3437–3447 (2006).
36. G. Gadda, Oxygen activation in flavoprotein oxidases: the importance of being positive. *Biochemistry* **51**, 2662–2669 (2012).
37. T. Domratcheva, Neutral histidine and photoinduced electron transfer in DNA photolyases. *J. Am. Chem. Soc.* **133**, 18172–18182 (2011).
38. K. F. Biegasiewicz, *et al.*, Photoexcitation of flavoenzymes enables a stereoselective radical cyclization. *Science* **364**, 1166–1169 (2019).
39. E. J. Land, A. J. Swallow, One-electron reactions in biochemical systems as studied by pulse radiolysis. II. Riboflavin. *Biochemistry* **8**, 2117–2125 (1969).
40. W. W. Parson, *Modern optical spectroscopy: with exercises and examples from biophysics and biochemistry,* (Springer, Berlin, ed. 2, 2015).
41. T. Tsuneda, J. W. Song, S. Suzuki, K. Hirao, On Koopmans' theorem in density functional theory. *J. Chem. Phys.* **133**, 174101 (2010).
42. P. S. Rao, M. Simio, E. Hayon, M. Slmic, Pulse radiolysis study of imidazole and histidine in water. *J. Phys. Chem.* **79**, 1260–1263 (1975).
43. C. Hao, J. L. Seymour, F. Tureček, Electron super-rich radicals in the gas phase. a neutralization-reionization mass spectrometric and ab Initio/RRKM study of diaminohydroxymethyl and triaminomethyl radicals. *J. Phys. Chem. A* **111**, 8829–8843

(2007).
44. G. Wohlfahrt, *et al.*, 1.8 and 1.9 Å resolution structures of the Penicillium amagasakiense and Aspergillus niger glucose oxidases as a basis for modelling substrate complexes. *Acta Crystallogr. Sect. D Biol. Crystallogr.* **55**, 969–977 (1999).
45. J. P. Roth, J. P. Klinman, Catalysis of electron transfer during activation of O2 by the flavoprotein glucose oxidase. *Proc. Natl. Acad. Sci. U. S. A*. **100**, 62–67 (2003).
46. C. Sanner, P. Macheroux, H. Rüterjans, F. Müller, A. Bacher, 15N- and 13C-NMR investigations of glucose oxidase from Aspergillus niger. *Eur. J. Biochem.* **196**, 663–672 (1991).
47. D. An, *et al.*, Shuffling active site substate populations affects catalytic activity: the case of glucose oxidase. *ACS Catal.* **7**, 6188–6197 (2017).
48. M. Faraggi, Y. Tal, The reaction of the hydrated electron with amino acids, peptides, and proteins in aqueous solution. II. Formation of radicals and electron transfer reactions. *Radiat. Res.* **62**, 347–356 (1975).
49. M. Namazian, M. L. Coote, Accurate calculation of absolute one-electron redox potentials of some para-quinone derivatives in acetonitrile. *J. Phys. Chem. A*. **111**, 7227–7232 (2007).
50. H. Neugebauer, F. Bohle, M. Bursch, A. Hansen, S. Grimme, Benchmark study of electrochemical redox potentials calculated with semiempirical and DFT methods. *J. Phys. Chem. A* **124**, 7166–7176 (2020).
51. H. Ishikita, E. W. Knapp, Redox potential of quinones in both electron transfer branches of photosystem I. *J. Biol. Chem.* **278**, 52002–52011 (2003).
52. A. Mattevi, *et al.*, Crystal structure of D-amino acid oxidase: a case of active site mirror-image convergent evolution with flavocytochrome b2. *Proc. Natl. Acad. Sci. U. S. A.* **93**, 7496–7501 (1996).
53. M. Ghanem, G. Gadda, On the catalytic role of the conserved active site residue His 466 of choline oxidase. *Biochemistry* **44**, 893–904 (2005).
54. A. M. Orville, G. T. Lountos, S. Finnegan, G. Gadda, R. Prabhakar, Crystallographic, spectroscopic, and computational analysis of a flavin C4a−oxygen adduct in choline oxidase. *Biochemistry* **48**, 720–728 (2009).
55. D. Hamdane, V. Guérineau, S. Un, B. Golinelli-Pimpaneau, A catalytic intermediate and several flavin redox states stabilized by folate-dependent tRNA methyltransferase from Bacillus subtilis. *Biochemistry* **50**, 5208–5219 (2011).
56. P. Sournia, thesis, École polytechnique, Palaiseau, France (2016).
57. O. Quaye, S. Cowins, G. Gadda, Contribution of flavin covalent linkage with histidine 99 to the reaction catalyzed by choline oxidase. *J. Biol. Chem.* **284**, 16990–16997 (2009).
58. G. Williamson, D. E. Edmondson, Effect of pH on oxidation-reduction potentials of 8.alpha.-N-imidazole-substituted flavins. *Biochemistry* **24**, 7790–7797 (2002).
59. A. Hassan-Abdallah, G. Zhao, Z. Chen, F. S. Mathews, M. S. Jorns, Arginine 49 is a bifunctional residue important in catalysis and biosynthesis of monomeric sarcosine oxidase: a context-sensitive model for the electrostatic impact of arginine to lysine mutations. *Biochemistry* **47**, 2913–2922 (2008).
60. A. Hense, E. Herman, S. Oldemeyer, T. Kottke, Proton transfer to flavin stabilizes the signaling state of the blue light receptor plant cryptochrome. *J. Biol. Chem.* **290**, 1743–1751 (2015).
61. S. P. Laptenok, P. Nuernberger, A. Lukacs, M. H. Vos, in *Methods in molecular biology, fluorescence spectroscopy and microscopy: methods and protocols,* (Humana, New York, 2014), vol. 1076, pp. 321–336.
62. J. J. Snellenburg, S. P. Laptenok, R. Seger, K. M. Mullen, I. H. M. van Stokkum, Glotaran: a Java-based graphical user interface for the R Package TIMP. *J. Stat. Softw.* **49** (2012).
63. F. Neese, The ORCA program system. *Wiley Interdiscip. Rev. Comput. Mol. Sci.* **2**, 73–78 (2012).
64. J. C. Phillips, *et al.*, Scalable molecular dynamics with NAMD. *J. Comput. Chem.* **26**, 1781–1802 (2005).
65. M. J. Field, The pDynamo program for molecular simulations using hybrid quantum

chemical and molecular mechanical potentials. *J. Chem. Theory Comput.* **4**, 1151–1161 (2008).
66. B. R. Brooks, *et al.*, CHARMM: A program for macromolecular energy, minimization, and dynamics calculations. *J. Comput. Chem.* **4**, 187–217 (1983).
67. J. Fabian, TDDFT-calculations of Vis/NIR absorbing compounds. *Dyes Pigm.* **84**, 36–53 (2010).

Figures and Tables

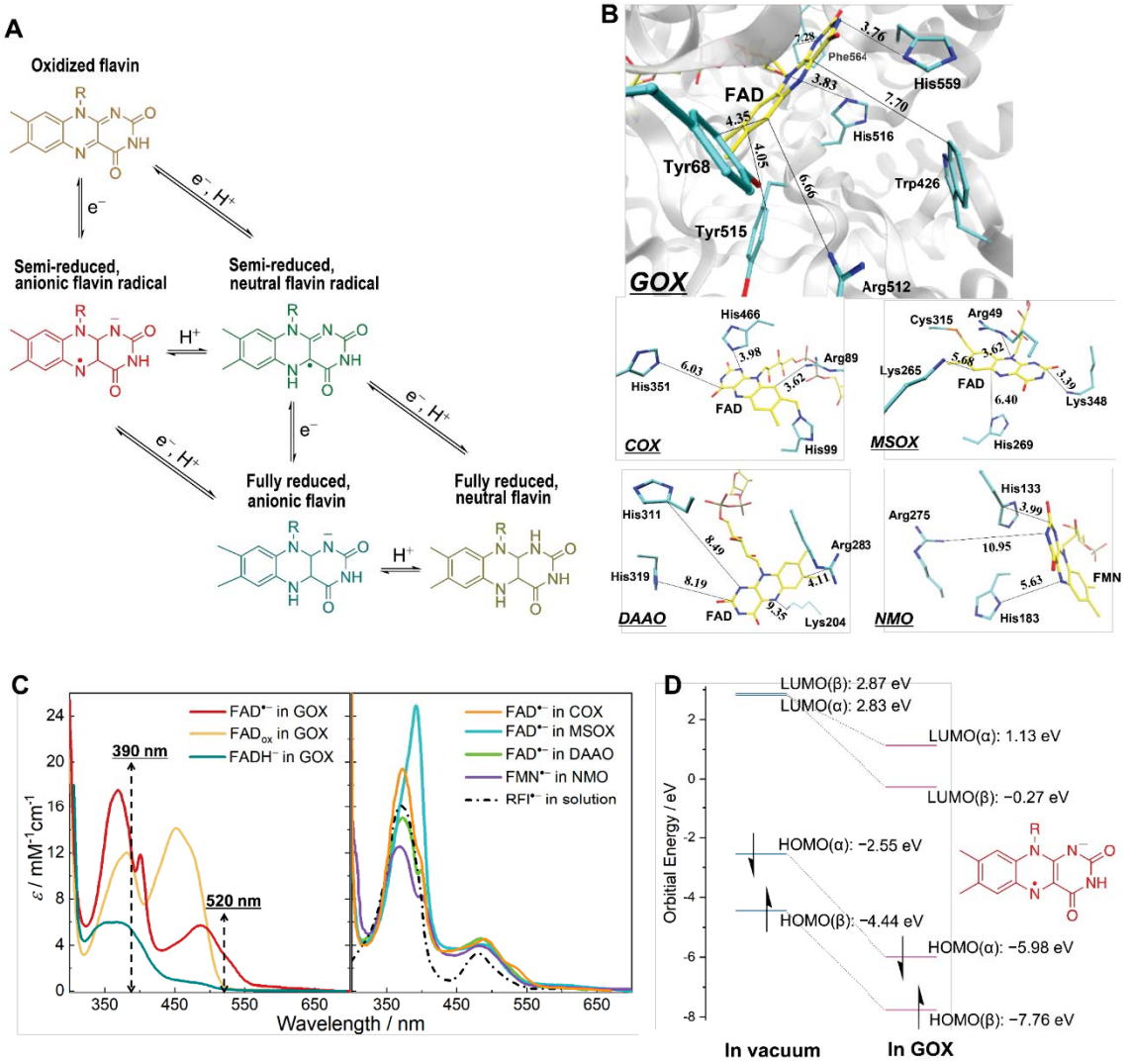

Figure 1. (*A*) Five redox and protonation states of flavins occurring as physiological reaction intermediates. Flavin is represented by the isoalloxazine moiety. (*B*) Active sites in the crystal structures of GOX from *Aspergillus niger* (PDB entry: 1CF3), COX from *Arthrobacter globiformis* (S101A variant; PDB entry: 3NNE), MSOX from *Bacillus sp.* (PDB entry: 2GB0), DAAO from porcine kidney (PDB entry: 1VE9; in complex with benzoate (not shown)), and NMO from *P. aeruginosa* PAO1 (PDB entry: 4Q4K). The carbon atoms of the flavin cofactors are shown in yellow, whereas those of selected active-site residues are displayed in cyan; nitrogen, oxygen and sulfur atoms are colored in blue, red and orange, respectively. The closest distances between flavin rings and non-hydrogen atoms of side chains are shown in Å. (*C*) Steady-state absorption spectra of flavin species in different systems. $FAD^{\bullet-}$ in GOX was generated by photoreduction in the presence of EDTA at pH 10.1, and the spectrum of FAD_{ox} in GOX was measured at pH 10.1. Spectra of $FAD^{\bullet-}$ in DAAO and $RFl^{\bullet-}$ in solution were reproduced from published data (25, 39). The other spectra were measured as described in *SI Methods*. For all the spectra, the reported values of extinction coefficients were used (25, 26, 29, 30). Dashed lines indicate the maxima of excitation

pulses in the time-resolved spectroscopic measurements. (*D*) HOMO and LUMO energy levels of $FAD^{\bullet-}$ calculated in vacuum and in GOX at the ωB97X-D3/ma-def2-TZVP level.

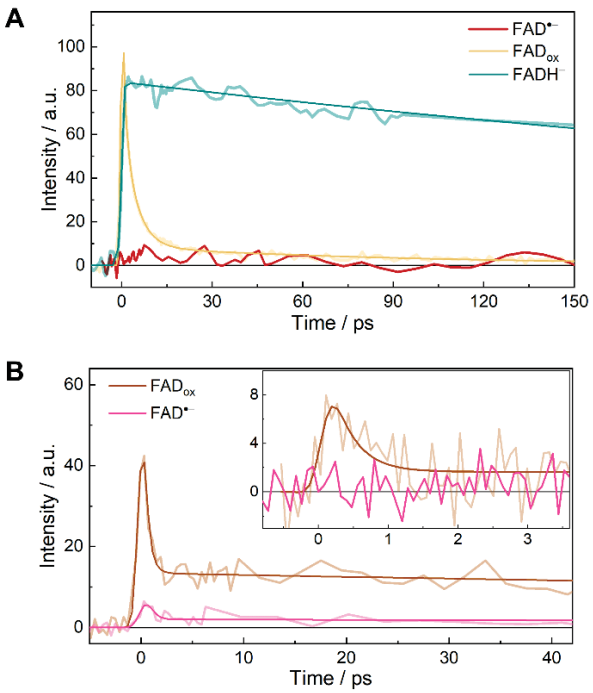

Figure 2. (*A*) Fluorescence decays of $FAD^{\bullet -}$, FAD_{ox}, and $FADH^{-}$ in GOX monitored at 537 nm under the same excitation conditions with CS_2 as the Kerr medium. Intensities were normalized based on the absorption of the samples at the excitation wavelength (390 nm). (*B*) Fluorescence decays of the as-prepared aerobic (FAD_{ox}) and reduced ($FAD^{\bullet -}$) samples of COX monitored at 532 nm, with benzene or suprasil (inset) as Kerr medium. Measurements were conducted with the same sample before and after the chemical reduction (see text). Exponential fits are shown as smooth curves.

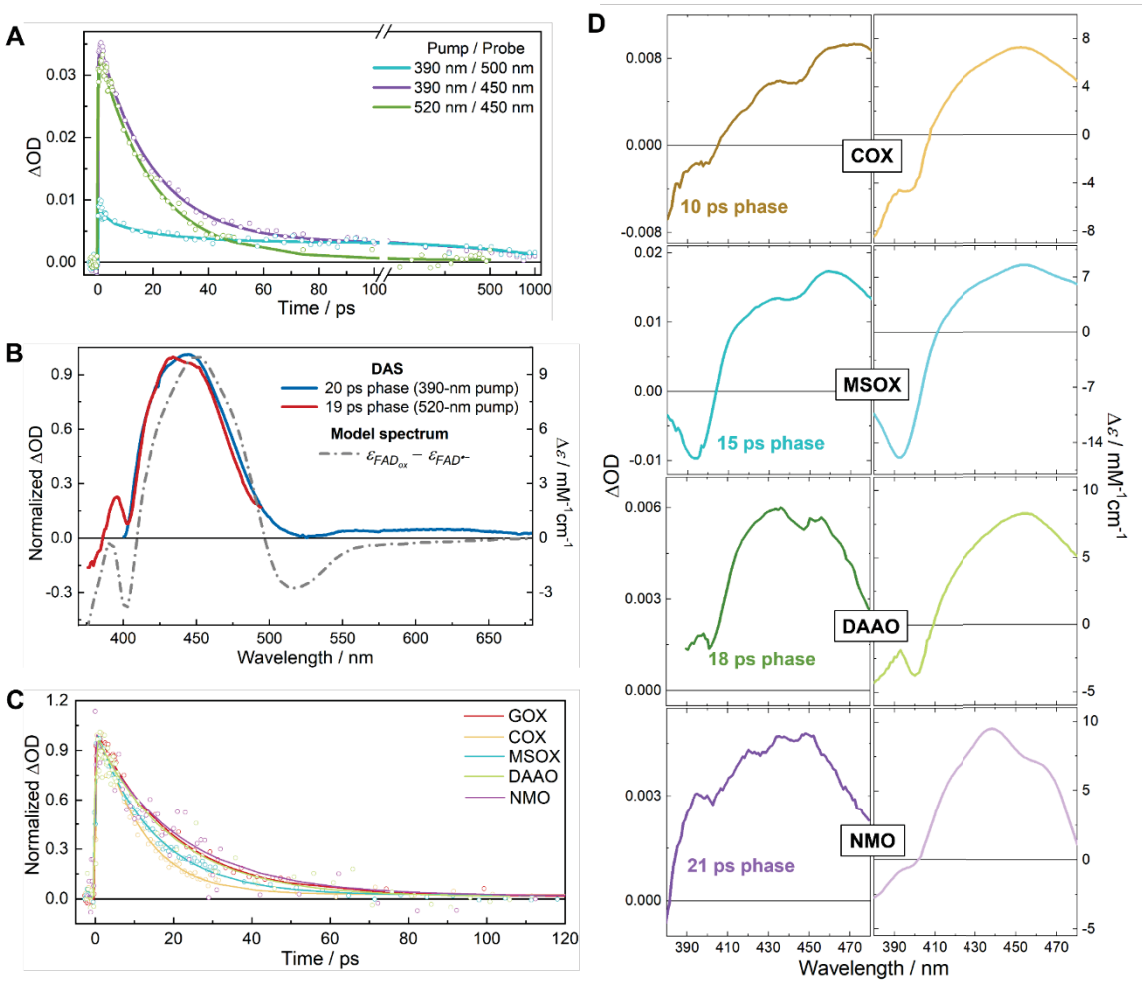

Figure 3. (*A*) Isotropic transient absorption kinetics of $FAD^{\bullet-}$ in GOX at selected wavelengths upon excitation at 390 nm or 520 nm. (*B*) Spectral analysis of DAS of $FAD^{\bullet-}$ in GOX under two excitation conditions. Model spectrum was constructed from steady-state spectra by assuming complete $FAD^{\bullet-}$ to FAD_{ox} conversion. (*C*) Isotropic transient absorption kinetics in different flavoprotein oxidases after excitation at 520 nm and monitored at 455 nm. (*D*) DAS of anionic flavin radicals in COX, MSOX, DAAO and NMO under excitation at 520 nm, as well as the corresponding steady-state difference spectra.

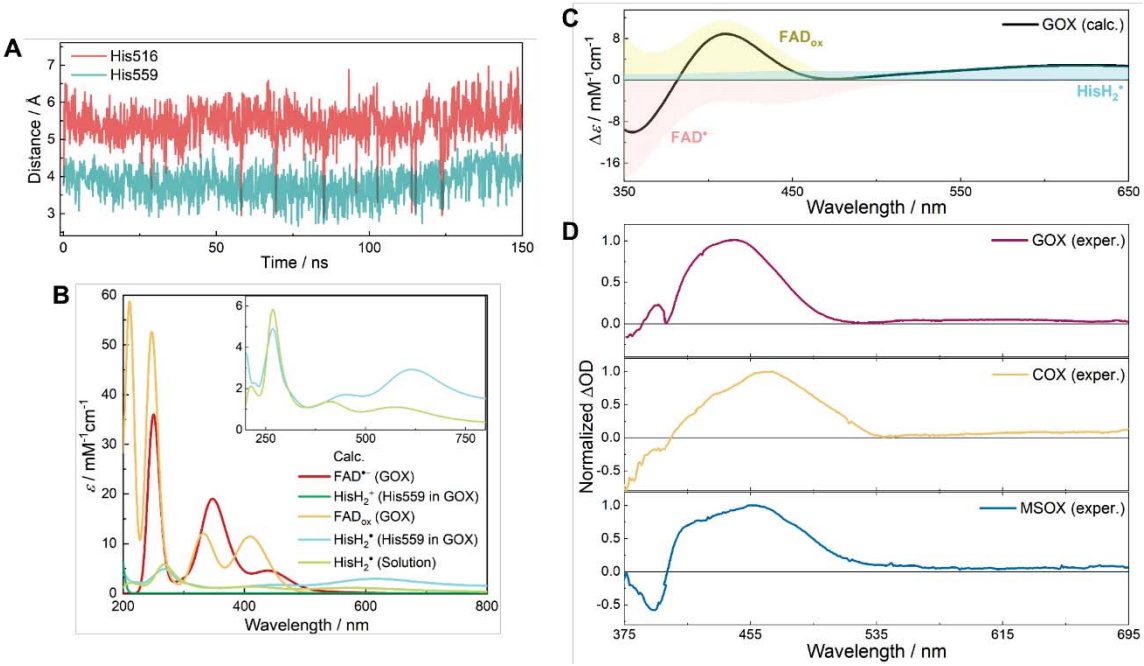

Figure 4. (*A*) The minimal ring-to-ring distance between $FAD^{\bullet-}$ and His516 or His559 in the MD simulation of GOX. (*B*) Calculated absorption spectra of individual species involved in the photooxidation process of $FAD^{\bullet-}$ in GOX. (*C*) Calculated transient spectrum of $FAD^{\bullet-}$ photooxidation in GOX by superimposing individual spectra of corresponding components in (B). (*D*) Experimental DAS of $FAD^{\bullet-}$ in GOX, COX and MSOX obtained by combining normalized DAS from two excitation conditions (375–420 nm: 520-nm pump, 420–695 nm: 390-nm pump; cf. Fig. 3B). Wavelength ranges of calculated and experimental spectra are different to account for a rigid shift arising from the limitation of calculations (10, 67).

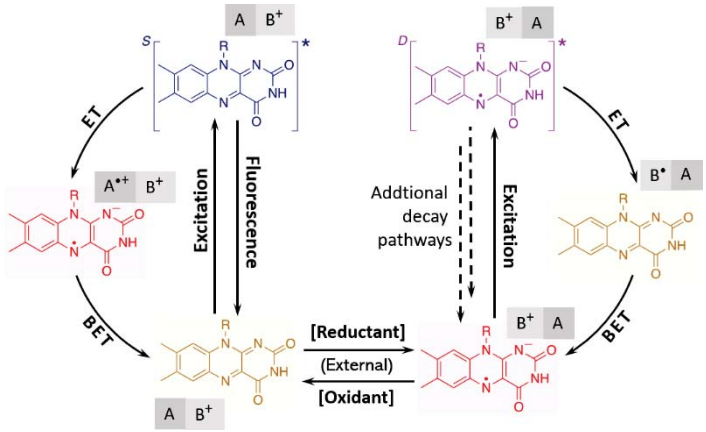

Figure 5. General reaction pathways for light-induced processes in flavoproteins that include the photooxidation of the anionic flavin radical. Flavin is represented by the isoalloxazine moiety. A stands for the electron-donating residue (tryptophan or tyrosine) and B^+ represents the electron-accepting residue (presumably histidine or arginine) in the protein active site.

PNAS
www.pnas.org

Supplementary Information for
Ultrafast Photooxidation of Protein-Bound Anionic Flavin Radicals

Bo Zhuang, Rivo Ramodiharilafy, Ursula Liebl, Alexey Aleksandrov*, and Marten H. Vos*

LOB, CNRS, INSERM, École Polytechnique, Institut Polytechnique de Paris, 91128 Palaiseau, France

*Alexey Aleksandrov

Email: alexey.aleksandrov@polytechnique.edu

*Marten H. Vos

Email: marten.vos@polytechnique.edu

This PDF file includes:

Supplementary Information Text

SI Methods

Sample Preparations.

GOX from *Aspergillus niger*, COX from *Arthrobacter sp.*, MSOX from *Bacillus sp.* and DAAO from porcine kidney were purchased from Sigma-Aldrich. GOX, COX and MSOX were used without further purification. DAAO from Sigma-Aldrich contained substantial excess free flavin, which was removed before use by washing with excess buffer followed by concentrating with a 30-kDa cutoff Amicon Ultra 4 filter (Millipore) three times (cf. Ref. (1)). The gene *pa4202* from *Pseudomonas aeruginosa* PAO1, coding for NMO, was inserted into plasmid pQE60 (Qiagen) via unique *NcoI* and *BamHI* restriction sites. The construct, carrying a hexahistidine (6xHis)-tag at its carboxyl terminus, was confirmed by DNA sequencing. Expression of the recombinant NMO protein in *E. coli* BL21DE3 was induced by adding 1 mM IPTG to early exponential phase cultures. 6xHis-tagged proteins were purified from cell-free extracts by gravity-flow chromatography on Ni-TED columns (Macherey Nagel), followed by subsequent imidazole removal as described previously (2).

Unless stated otherwise, phosphate buffer (~50 mM) was used for the pH range from 5.5 to 8.5, glycine-NaOH buffer (~80 mM) was used for the pH range from 9.0 to 13.0, and protein samples were prepared with a flavin concentration of 100–200 μM in 1-mm path length quartz cells. Flavins in the oxidized form were studied under aerobic conditions. Anionic flavin radicals were obtained in extensively degassed samples, either by chemical reduction or photoreduction. At pH 7.6, pH 10.1 or pH 13.0, to generate $FAD^{\bullet-}$ in GOX, FAD_{ox} was reduced by a 2-fold molar excess of sodium dithionite ($Na_2S_2O_4$) under anaerobic conditions. The photoreduction of GOX into the $FAD^{\bullet-}$ form was carried out as follows: the protein sample solution at pH 10.1 and in the presence of 10 mM EDTA or 1 mM 2-mercaptoethanol (2-ME) was irradiated by a 450 nm LED (0.45 W) for 90 minutes in an ice-bath (1, 3). $FADH^-$ in GOX was prepared by reduction under anaerobic conditions with a large excess of D(+)-glucose at pH 7.6. To obtain $FAD^{\bullet-}$ in COX, a 1.2-fold molar excess of $Na_2S_2O_4$ was added to the oxidized protein sample at pH 8.1 under anaerobic conditions, and the mixture was incubated at room temperature for 2 hours. $FAD^{\bullet-}$ in MSOX was prepared by reduction with a 2-fold molar excess of $Na_2S_2O_4$ at pH 8.5. $FAD^{\bullet-}$ in DAAO was produced by photoreduction in the presence of 1 mM 2-ME via a process similar to that described above for GOX, with an illumination time of 5 minutes. To obtain $FMN^{\bullet-}$ in NMO, reduction of NMO with propionate 3-nitronate was conducted in Tris-buffered saline (TBS) buffer at pH 8.0 as described in Ref. (4). The reduction processes were followed by monitoring steady-state absorption spectra with a Shimadzu UV–Vis 1700 spectrophotometer or fluorescence spectra with a Cary Eclipse fluorometer. The experimental conditions for preparing reduced flavins are also summarized in Table S1.

Spectroscopic Measurements.

The setup for time-resolved fluorescence employs a Kerr gate (5). Briefly, part of the 780 nm output from the Ti:sapphire laser/amplifier system (Quantronix Integra-C) operating at 0.5 kHz was passed through a BBO crystal, yielding an excitation pulse centered at 390 nm. The remaining 780 nm beam was directed through a motorized delay-line and focused into the Kerr medium where it spatially overlapped the fluorescence from the sample. Kerr media with different time-resolution/sensitivity compromises were used, i.e., suprasil (response time ~200 fs), benzene (response time ~400 fs) and CS_2 (response time ~1 ps).

Multicolor time-resolved absorption spectra were recorded by the pump–probe technique on an instrument operating at 500 Hz, as described previously (2, 6). Pump pulse centered at 390 nm were obtained by frequency-doubling the fundamental beam. Pump pulses centered at 520 nm were obtained with a non-collinear optical parametric amplifier and tailored with a sharp-edge interference filter. Continuum broadband pulses were used as the probe. Pump and probe beams were set at the magic angle (54.7°) to record the isotropic spectra. Additionally, parallel and perpendicular pump–probe configurations were used for recording the transient anisotropy data. The excitation power was adapted such that each shot of the pump beam excited less than 10% of the sample. The concentrations of excited molecules were determined using $[Ru(bpy)_3]Cl_2$ as a reference (6), as detailed in *Note 4*. Unless indicated otherwise, for reduced protein samples, those reduced chemically were used in time-resolved spectroscopic measurements, and all the

measurements were carried out at 10 °C. Global analysis of the data was performed using the Glotaran program based on the R-package TIMP (7).

Computer Simulations.

Geometry optimizations in vacuum were performed at the ωB97X-D3/ma-def2-TZVP level (8, 9). Vibrational analysis was performed on the optimized structures to confirm that the optimization converged to a minimum. To calculate the free energy changes of redox reactions, single point energies were calculated on the optimized geometries at the PWPB95-D4/def2-QZVPP level, as suggested in Ref. (10), while the thermostatistical corrections at 298.15 K were obtained from the frequency analysis at the ωB97X-D3/ma-def2-TZVP level. The SMD solvation model (11) was used to estimate the solvation energies in the aqueous solution at the M06-2X/6-31G* level (12). These DFT calculations were carried out using the ORCA program (version: 4.2) (13).

MD simulations of GOX were carried out using the NAMD programs (version 2.13) (14). The structure of GOX from *Aspergillus niger* was taken from the Protein Data Bank (PDB entry: 1CF3). The CHARMM36m force field was used for the protein residues (15) and the TIP3P model for water (16); a recently developed force field for flavins was used to describe $FAD^{\bullet-}$ and $FADH^{-}$ (17). The protonation states of all titratable residues other than His516 were assigned based on a PROPKA 3.1 analysis (18), and verified by ideal stereochemistry. The pK_a value of His516 in the active site of GOX and in the presence of $FAD^{\bullet-}$ or $FADH^{-}$ was specifically calculated using computationally intensive MDFE simulations (19), as described in *Note 6*. A disulfide bridge was created between Cys164 and Cys206. The protein was placed in a cubic water box, at least 12 Å away from each of the box faces. Periodic boundary conditions were assumed, and an appropriate number of potassium counterions was included to neutralize the net charge of the system. Long-range electrostatic interactions were computed using the particle mesh Ewald method (20). The integration time step was set at 2 fs. After energy minimization, the system was equilibrated first in an NVT ensemble for 50 ps, followed by a 500 ps simulation in the NPT ensemble, at 295 K and 1.0 atm pressure before the production runs. The Berendsen thermostat and barostat were employed, with a relaxation time of 500 fs and 4 timesteps between position rescalings (21).

For GOX, the spectral properties of $FAD^{\bullet-}$ in the resting state, as well as transient FAD_{ox} and reduced His559 (in the neutral radical form, $HisH_2^{\bullet}$), were calculated via a QM/MM approach, using the pDynamo program (version 1.9.0) (22) coupled with the ORCA package. 20 structures taken each 7.5 ns from the 150 ns MD trajectories were used for the QM/MM calculations. Electrostatic interactions between the QM and MM regions were treated using the electrostatic embedding. The QM region included the isoalloxazine ring moiety of FAD or the side chain of His559, with the remaining groups of FAD, protein residues and water molecules (580 protein residues and 20061 water molecules) included to the MM region and described with the same force fields as in the MD simulations (Fig. S22). To model the product state following the photooxidation reaction, at the MM level, the force field parameters of FAD were modified to correspond to FAD_{ox} (17) and those of His559 to $HisH_2^{\bullet}$. In particular, the CHELPG atomic charges (23) for $HisH_2^{\bullet}$ were obtained by fitting the QM electrostatic potential around the solutes after geometry optimizations in vacuum at the QM level (ωB97X-D3/ma-def2-TZVP, Table S6). For the bonded terms in the force field model, we used those from the standard force fields of doubly protonated histidine, as justified in Ref. (6, 24) The QM region was first optimized by energy minimization with the MM regions fixed using the L-BFGS optimization method at the (U)B3LYP/6-31+G* level (25, 26), with a RMS gradient tolerance of 0.2 kcal/(mol Å) as the convergence criterion. Excitation energies and oscillator strengths of 30 excited states were then estimated using TDDFT calculations performed at the same QM level. The results of all snapshots were broadened with a Gaussian line shape (FWHM: 0.42 eV) and then averaged.

HOMO and LUMO energy levels of $FAD^{\bullet-}$ were calculated in a vacuum and in GOX. Those in a vacuum are based on the geometry optimized at the ωB97X-D3/ma-def2-TZVP level, while in GOX the calculations were performed at the ωB97X-D3/ma-def2-TZVP level considering the effects of the protein environment, based on QM/MM-optimized geometries at the UB3LYP/6-31+G* level, and averaged for 20 snapshots along the MD trajectories to give the results shown in Fig. 1D of the main text.

The PB equation was solved using the CHARMM program (version: 45b2) (27) to evaluate electrostatic energies in the protein-water systems. The dielectric constant was set to 2 inside the protein and 80 for water. The protein dielectric constant was higher than 1 to include implicitly the electronic relaxation, which is absent in the additive C36 force field (28). The PB energies were computed using the focusing method with a coarse grid of 0.8 Å resolution and a fine grid with 0.4 Å resolution, based on the coordinates of 100 snapshots taken each 1.5 ns from the MD trajectories. The partial charges in the MM region of the model were set accordingly to represent the system before and after the ET reaction. Combined with the calculations of redox free energy changes in solution based on the DFT calculations described above, the change of free energy due to the ET reaction in the protein environment can be estimated (*Note 7*).

Note 1. Steady-state reduction of oxidized flavins

The experimental conditions for preparing reduced flavin species in this study are summarized in table S1. The results are similar to those reported in the literature (as an illustration, the process of reduction of FAD_{ox} in COX by $Na_2S_2O_4$ is given in the inset of Fig. S2), except for $FAD^{\bullet-}$ in DAAO. During the photoreduction of DAAO, when the reaction reached the maximum radical formation (judged by whether pursuing the illumination would reduce the overall absorbance in the visible range, which is an indication of accumulation of fully reduced flavins), we obtained a spectrum that appears to have a FAD_{ox} contribution (Fig. S3). This is most likely due to residual free flavin present in our sample (a commercial product purchased from Sigma and subsequently purified by repeated washing steps with excess buffer), which after illumination is present in an equilibrium between the oxidized and fully reduced forms because the redox potentials for the oxidized/semi-reduced and semi-reduced/fully-reduced couples of free flavins in solution are close. We also attempted photoreduction of DAAO purchased from Abnova, which did not contain excess free flavin. However, it appeared unstable in solution.

Previous reports by Massey *et al.* have proposed that the photoreduction of oxidized flavins in flavoproteins occurs mostly via an exchange of electrons between a trace amount of fully reduced free flavin in solution and protein-bound oxidized flavin, involving equilibria between oxidized, semi-reduced and fully reduced forms (29, 30). Given this mechanism, it might be difficult to achieve a 100%-yield formation of the anionic radical form, as trace amounts of oxidized flavin, fully reduced flavin, or even unknown residue–flavin adducts (see below) can remain present in the sample. This can complicate the time-resolved measurements under 390-nm excitation, because those flavin species usually absorb in the near ultraviolet range (Fig. 1C of the main text, Fig. S9).

Note 2. Fluorescence of flavin species in GOX and COX

Fluorescence of flavin species in COX exhibits complex behaviors. For the as-prepared COX sample under oxidizing conditions, time-resolved fluorescence measurements show that its fluorescence decays in a biphasic manner with an ultrafast 300-fs phase and a relatively long-lived 440-ps phase (Fig. S7a, Table S2). In the active site of COX, there are electron-donating residues, Tyr465 and Trp61, located close to the flavin (Fig. S10). Therefore, the 300-fs phase can be assigned to the fluorescence of FAD_{ox} quenched by ultrafast photoinduced ET from those nearby residues, which is a phenomenon commonly observed in flavoproteins (24, 31, 32). On the other hand, steady-state fluorescence excitation and emission spectra (Fig. S9), which essentially reflect the integrated fluorescence of the long-lived phase in the time-resolved measurements, clearly demonstrate that the 440-ps phase results from a species different from FAD_{ox}, with an absorption maximum at ~400 nm. The spectral features of this unknown species highly resemble those of a residue–flavin adduct in COX obtained at a high pH, which has been proposed to be a C4a-N-histidyl-FAD adduct (33).

For the reduced COX sample, as discussed in the main text and illustrated in Fig. S7, in the time-resolved measurements, the reduction reaction appears to diminish the overall intensities of the fluorescence rather than result in different spectra and dynamics. The steady-state fluorescence spectra (Fig. S8) further confirm that the integrated fluorescence observed under 400-nm excitation

cannot be due to $FAD^{\bullet-}$, as we did not observe any emission when exciting the sample at 500 nm where $FAD^{\bullet-}$ absorbs.

Altogether, we ascribe the fluorescence detected in the reduced COX sample to a trace amount of FAD_{ox} (290-fs phase) and the residue–flavin adduct or other unidentified reaction by-products (320-ps phase) present in the sample. Any emission from $FAD^{\bullet-}$ must decay on a much shorter timescale, exceeding the temporal resolution of our measurements.

Note 3. Transient absorption measurements under different conditions

The transient absorption spectra of $FADH^-$ in GOX (Fig. S11, S12) are consistent with those reported in the literature (34). As discussed in the main text, the spectral features and dynamics of excited-state $FADH^-$ resemble the long-lived phase of $FAD^{\bullet-}$ in GOX (Fig. S13), indicating that the complexity of the transient absorption spectra of $FAD^{\bullet-}$, with two additional small phases under 390-nm excitation, can be attributed to the presence of a trace amount of other flavin species in a different redox state. This may also be the case for COX and MSOX (Fig. S14, S15), as we have demonstrated above a slightly inhomogeneous composition of the reduced sample for these species. For MSOX, the spectral features of the 1.7 ps phase (Fig. S15) are indeed very similar to what we have observed upon excitation of FAD_{ox} at 390 nm (data not shown).

As shown in Fig. S16, $FAD^{\bullet-}$ in GOX prepared via different methods or at different pH exhibits similar transient absorption spectra. Yet, the overall shapes of the ~20-ps phases of the different samples slightly vary, whereas the ground-state absorption spectrum of FAD_{ox} in GOX does not perceptibly depend on the pH (Fig. S17). This suggests that the spectral properties of the transiently formed FAD_{ox} (or the electron acceptor species) are sensitive to the local protein environment on an ultrafast timescale. The variation in relative amplitudes of the ~2 ps and ~ns phases might reflect variation in the yields of $FAD^{\bullet-}$ under different conditions.

Note 4. Determination of the initial concentrations for transient species

Using $[Ru(bpy)_3]Cl_2$ as a reference, we determined the initial concentrations of excited $FAD^{\bullet-}$ in GOX in transient absorption measurements. Under the same excitation conditions, we have (24, 35):

$$c^*_{FAD^{\bullet-}} = \frac{c^*_{Ru}\left(1-10^{-A^{gs}_{FAD^{\bullet-}}}\right)}{1-10^{-A^{gs}_{Ru}}} \qquad (\mathrm{eq.\,s1})$$

where $c^*_{FAD^{\bullet-}}$ is the concentration of excited $FAD^{\bullet-}$, $\underline{c^*_{Ru}}$ is the concentration of the excited Ru complex, $A^{gs}_{FAD^{\bullet-}}$ and A^{gs}_{Ru} are the ground-state absorbance of $FAD^{\bullet-}$ in GOX, and the $[Ru(bpy)_3]^{2+}$ sample at the excitation wavelength, respectively.

Upon excitation, $[Ru(bpy)_3]^{2+}$ undergoes a charge transfer reaction resulting in a long-lived metal-to-ligand charge transfer (MLCT) state. The reaction has a 100% quantum yield and the difference of molar extinction coefficient of $[Ru(bpy)_3]^{2+}$ at 450 nm following this reaction ($\Delta\varepsilon_{450}$) has been reported to be $-1.1 \times 10^4\ M^{-1}cm^{-1}$ (36). Therefore, c^*_{Ru} can be calculated from a reference transient absorption measurement, and used to estimate $c^*_{FAD^{\bullet-}}$ according to eq. s1. Using this approach, in our measurement of GOX, $c^*_{FAD^{\bullet-}}$ is estimated to be 2.2×10^{-2} mM. Alternatively, by assuming a photooxidation reaction with 100% yield, $c^*_{FAD^{\bullet-}}$ can also be estimated from the initial amplitude (at 450 nm) of the product state, by dividing it with the difference of ground-state extinction coefficients $(\varepsilon_{FAD_{ox}} - \varepsilon_{FAD^{\bullet-}})_{450}$, which gives a value of 2.7×10^{-2} mM. The fact that the difference between the two estimations is small further supports the assumption of a photooxidation reaction with near-unity yield. It is also worth noting that the latter calculation may overestimate the concentration if a third species contributes to the transient absorption spectra in the probed region, which is very likely to be the case here.

Note 5. Calculations of anisotropy and orientation of transition dipole moments

In transient anisotropy experiments, the transient absorption spectra are measured with the pump and probe pulses polarized parallel ($\Delta A_{\parallel}$) and perpendicular ($\Delta A_{\perp}$) (37). For pumping and probing single transitions, the anisotropy *r*:

$$r = \frac{\Delta A_{\parallel} - \Delta A_{\perp}}{\Delta A_{\parallel} + 2\Delta A_{\perp}} \qquad (\text{eq. s2})$$

It is related to the angle ϕ between the pumped and probed transition as:

$$r = \frac{3cos^2\phi - 1}{5} \qquad (\text{eq. s3})$$

For pumping and probing identical or parallel transitions (ϕ = 0), *r* can be calculated to be 0.4 according to eq. s3.

To obtain a theoretical prediction for the transition dipole moments of an anionic flavin radical, the structure of its chromophore (lumiflavin) in the anionic radical form was optimized at the ωB97X-D3/ma-def2-TZVP level in a vacuum, and then TDDFT calculations were performed based on the optimized structure at the PEB0/ma-def2-TZVP level for 30 excited states. The result (Fig. S19) demonstrates that the two major transient bands of the anionic flavin radical in the visible/near ultraviolet range ($D_0 \rightarrow D_4$ and $D_0 \rightarrow D_6$) form a small angle (8°), which is qualitatively consistent with our experimental observations.

Note 6. MDFE simulations for pK_a calculations

The pK_a of a titratable group in the protein environment can be calculated by:

$$\mathrm{p}K_{\mathrm{a,prot}} = \mathrm{p}K_{\mathrm{a,ref}} + \frac{\Delta\Delta G}{2.303RT} \qquad (\text{eq. s4})$$

where p$K_{a,prot}$ and p$K_{a,ref}$ are the pK_a of the titrating group in the protein and the reference model compound in the solution, respectively, and $\Delta\Delta G = \Delta G_{\mathrm{prot}} - \Delta G_{\mathrm{solv}}$ is the double free energy difference (19, 38).

To calculate $\Delta\Delta G$ we use alchemical free energy simulations (39), where the system of interest is gradually transformed from the initial state A to the final state B by modifying the energy function *U*, and the simplest scheme is to make *U* a linear function of the coupling parameter, λ:

$$U(\lambda) = (1-\lambda)U_{\mathrm{A}} + \lambda U_{\mathrm{B}} \qquad (\text{eq. s5})$$

where U_A and U_B are the energy functions of the initial and final states. A value between 0 and 1 corresponds to a hybrid system which is a mixture of A and B. The corresponding free energy was then obtained by thermodynamic integration (TI):

$$\Delta G = \int_0^1 \langle \frac{\partial U(\lambda)}{\partial \lambda} \rangle_{\lambda} \, d\lambda \qquad (\text{eq. s6})$$

Based on the MDFE method described above, we calculated the pK_a value of His516 in GOX in the presence of $FAD^{\bullet-}$ or $FADH^-$. The MD were performed with the NAMD program (14). In particular, protein residues within a 24 Å sphere centered at the isoalloxazine ring of FAD were placed in cubic water boxes, at least 12 Å away from each of the box edges, similar to our previous studies (40, 41). Non-hydrogen atoms between 20 and 24 Å from the sphere center were harmonically restrained to their experimentally determined positions based on the crystal structure. The other settings of the system and the procedure of the equilibration run are similar to those described in for the full-protein MD simulation above. To perform free energy simulations, the λ values employed were 0.00, 0.25, 0.50, 0.75, and 1.00, and the charges in the force field were modified accordingly to represent the deprotonation process of histidine (where the N_ε was deprotonated). 20 individual runs were performed where Δ*G* was calculated every 50 ns, and the production MD sampling time accumulated to 1 ms in total. The derivatives in eq. s6 were computed numerically and averaged over 500 structures from a window simulation. MDFE simulations were performed for a dipeptide with a histidine side chain immersed in a 30-Å box of water to estimate the free energy change of histidine deprotonation in solution (ΔG_{solv}). The pK_a of His516 was then computed (experimental pK_a in solvent for His_ε: 7.0) according to eq. s4. The results of the MDFE simulations are summarized in Table S5. Calculations were performed in the presence of $FADH^-$ to verify the method, since the experimental pK_a value of His516 was measured previously with this

state of flavin, with a value of 8.1 determined by the reaction rates of the reduced enzyme toward O_2 (42). The result shows that, in the presence of $FADH^-$, the pK_a of His516 is calculated to be 9.6 (SD: 0.4), which is reasonably close to the experimental value.

Note 7. Calculation of free energy changes of redox processes

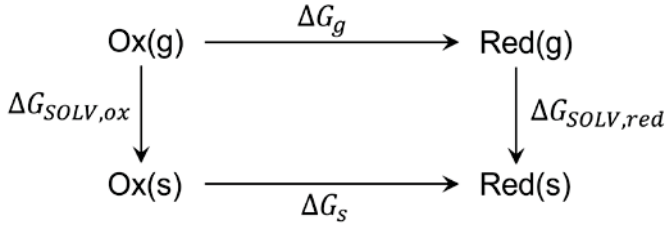

As shown in the scheme above, the change of free energy of the redox reaction in solvent, ΔG_s, can be calculated from its components by introducing a thermodynamic cycle:

$$\Delta G_s = \Delta G_g + \Delta G_{SOLV,red} - \Delta G_{SOLV,ox} \qquad (\mathrm{eq.s7})$$

$$\Delta G_g = G_{g,red} - G_{g,ox} - 2.5RT \qquad (\mathrm{eq.s8})$$

where $G_{g,red}$ and $G_{g,ox}$ are the energies of the redox pair in the gas phase, $\Delta G_{solv,ox}$ and $\Delta G_{solv,red}$ are solvation energies of the oxidized and reduced species in water, respectively, and the $2.5RT$ term corresponds to the thermal energy of the free electron (43).

Using the energies estimated by DFT calculations (Table S7), the change of free energy of the ET reaction, $FAD^{\bullet-}/HisH_2^+ \rightarrow FAD_{ox}/HisH_2^{\bullet}$, in aqueous solution, $\Delta G_{ET,solv}$, can be computed as:

$$\Delta G_{ET,solv} = \Delta G_{s,HisH_2^+/HisH_2^\bullet} - \Delta G_{s,FAD_{ox}/FAD^{\bullet-}} \qquad (\mathrm{eq.s9})$$

to be 189.1 kJ/mol or 1.96 eV.

In order to compute the change of free energy due to the ET reaction in the protein environment, the PB equation was solved using the following parameters. The dielectric constant was set to 2 inside the protein and 80 for water. The protein dielectric constant was higher than 1 to include implicitly the electronic relaxation, which is absent in the additive C36 force field (28). The PB energies were computed using the focusing method with a coarse grid of 0.8 Å resolution and a fine grid with 0.4 Å resolution. The partial charges in the MM region of the model were set accordingly to represent the system before and after the ET reaction. The difference of electrostatic energies of the systems before and after the ET reaction, $\Delta\Delta G_{ES}$, was then computed as:

$$\Delta\Delta G_{ES} = \Delta G_{ES,post} - \Delta G_{ES,pre} \qquad (\mathrm{eq.s10})$$

where $\Delta G_{ES,pre}$ and $\Delta G_{ES,\,post}$ are obtained from the solution of the PB equation (44). By performing the calculations on the structures of 100 snapshots taken each 1.5 ns from the MD trajectories of the GOX simulation, the average of $\Delta\Delta G_{ES}$ is calculated to be 5.3 (SD:1.1) kcal/mol or 0.23 (SD: 0.05) eV.

Supplementary Figures

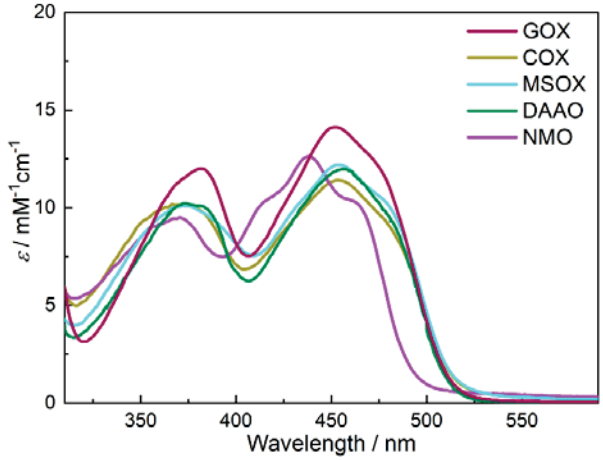

Fig. S1. Steady-state absorption spectra of oxidized flavins in GOX, COX, MSOX, DAAO and NMO under aerobic, non-reducing conditions.

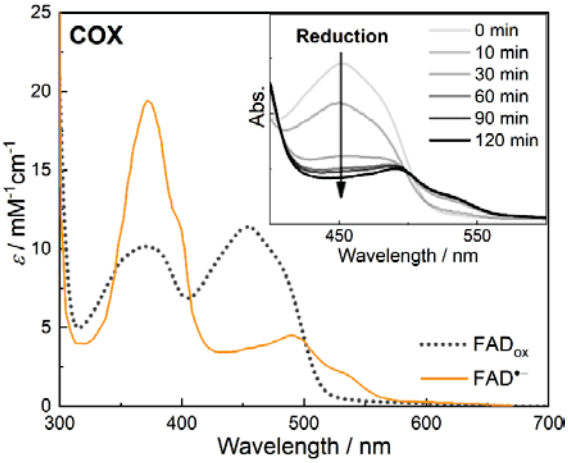

Fig. S2. Chemical reduction of FAD_{ox} and formation of $FAD^{\bullet-}$ in COX under anaerobic conditions. The inset shows the spectral changes recorded at different time points during the reduction process with $Na_2S_2O_4$.

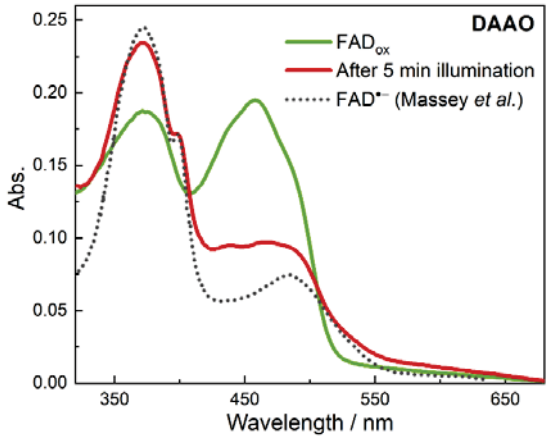

Fig. S3. Photoreduction of FAD_{ox} in DAAO in the presence of 2-ME. The illumination was stopped before the fully reduced flavin started to accumulate in the sample. The spectrum of $FAD^{\bullet-}$ in DAAO reported by Massey *et al.* (3) is shown as a dotted line for comparison.

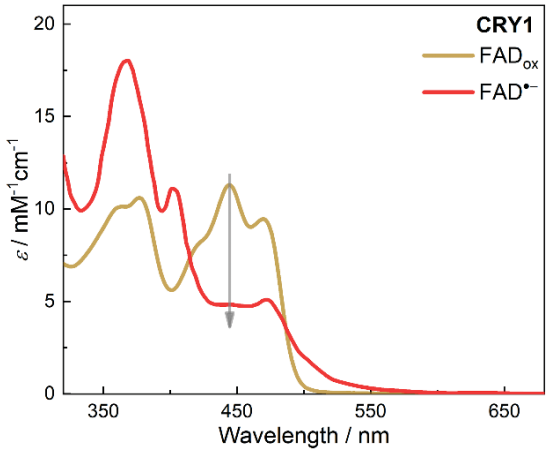

Fig. S4. Steady-state absorption spectra of FAD_{ox} and $FAD^{\bullet-}$ in insect cryptochrome (45).

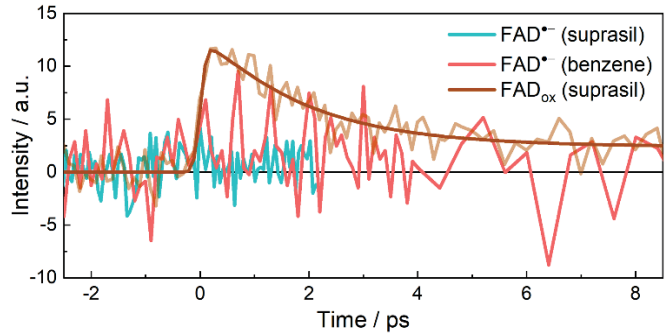

Fig. S5. Time-resolved fluorescence measurements of $FAD^{\bullet-}$ and FAD_{ox} in GOX with benzene or suprasil as Kerr medium.

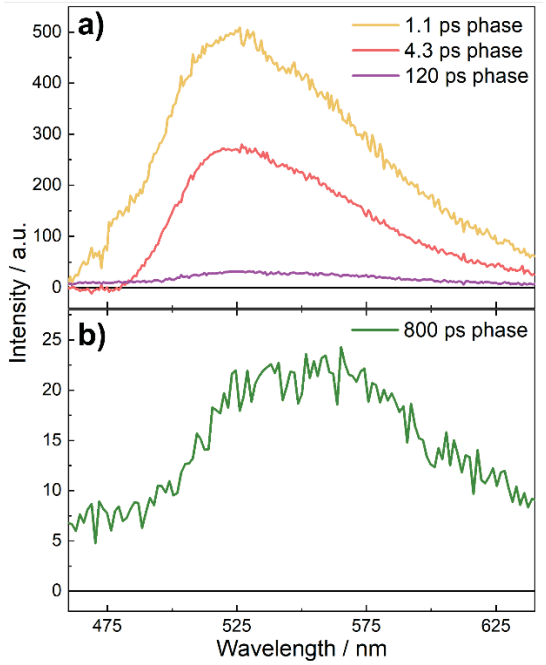

Fig. S6. DAS from the global analysis of fluorescence decays of FAD_{ox} (a) and $FADH^{-}$ (b) in GOX with CS_2 as Kerr medium.

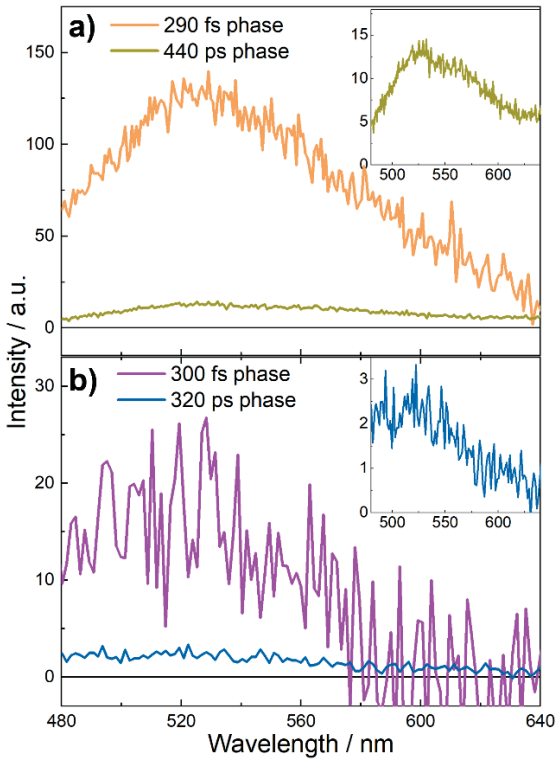

Fig. S7. DAS from the global analysis of fluorescence decays of COX under oxidizing (a) and reducing (b) conditions with benzene as Kerr medium.

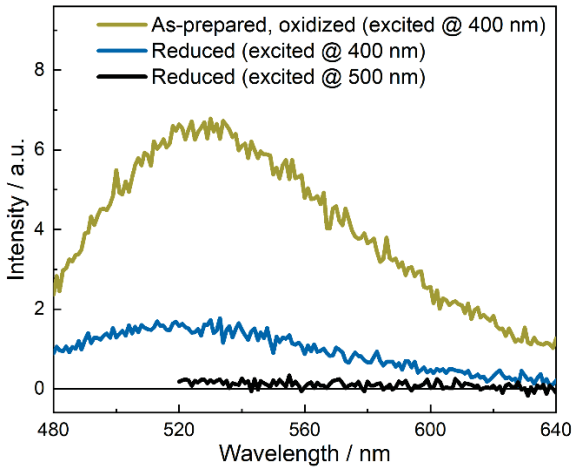

Fig. S8. Steady-state fluorescence of COX under oxidizing (a) and reducing (b) conditions.

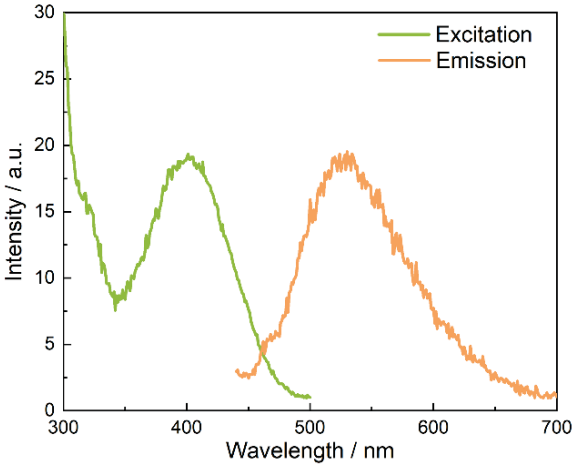

Fig. S9. Steady-state fluorescence excitation (monitored at 550 nm) and emission (excited at 400 nm) spectra of the as-prepared, oxidized sample of COX.

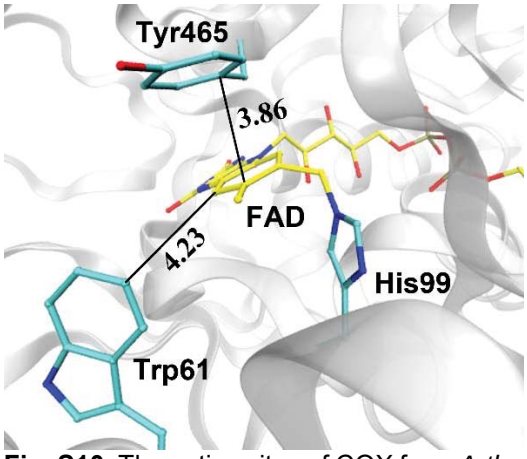

Fig. S10. The active sites of COX from *Arthrobacter globiformis* (S101A variant; PDB entry: 3NNE). The shortest ring-to-ring distances between the flavin and close-by electron-donating residues are shown in Å.

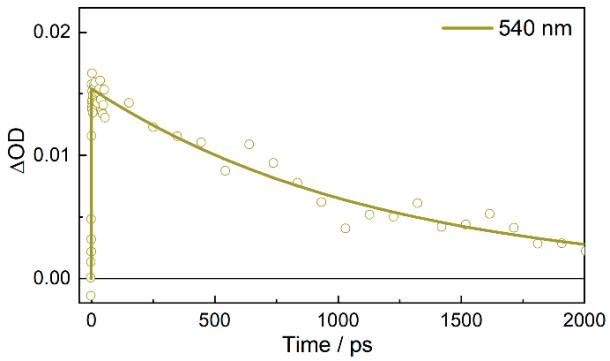

Fig. S11. Isotropic transient absorption kinetics of $FADH^-$ in GOX at 540 nm upon excitation at 390 nm.

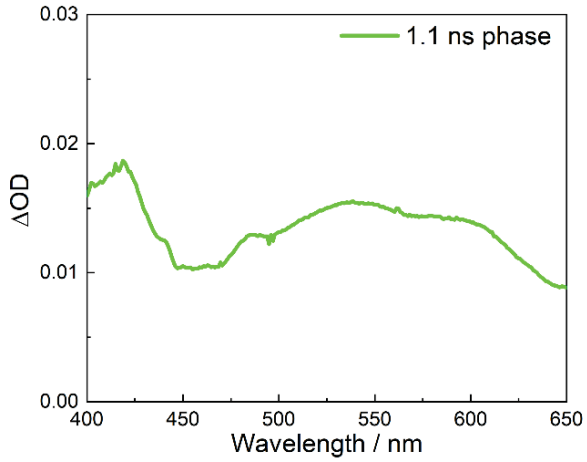

Fig. S12. DAS of isotropic transient absorption data of $FADH^-$ in GOX under excitation at 390 nm.

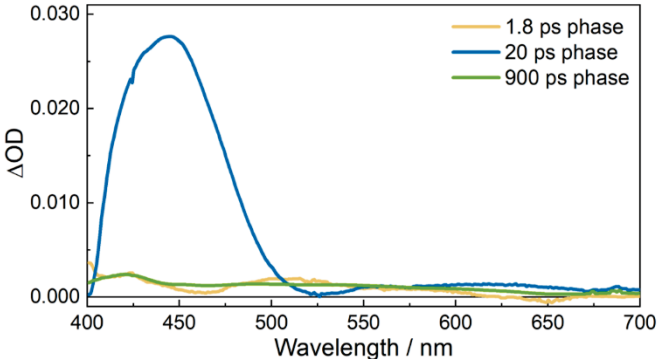

Fig. S13. DAS of isotropic transient absorption data of $FAD^{\bullet-}$ in GOX under excitation at 390 nm.

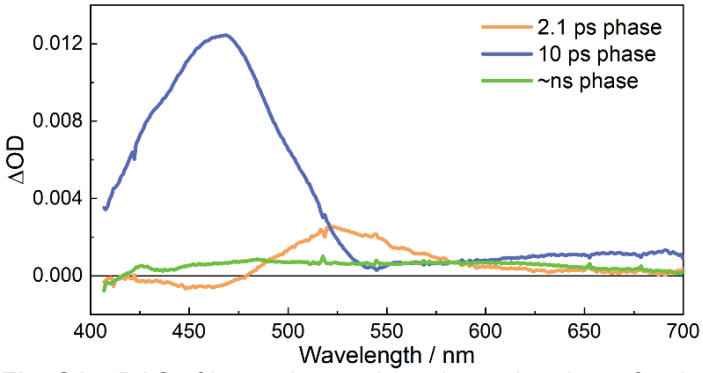

Fig. S14. DAS of isotropic transient absorption data of reduced COX under excitation at 390 nm.

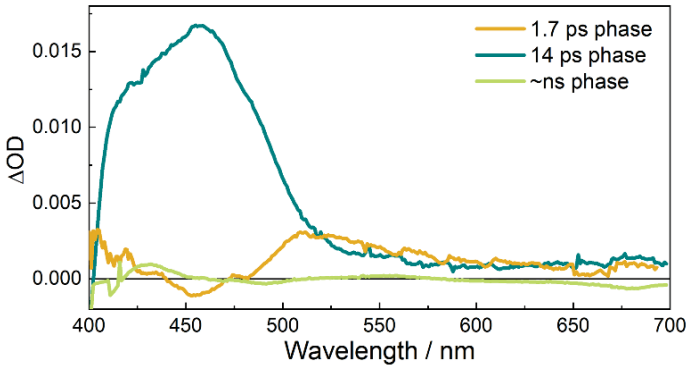

Fig. S15. DAS of isotropic transient absorption data of reduced MSOX under excitation at 390 nm.

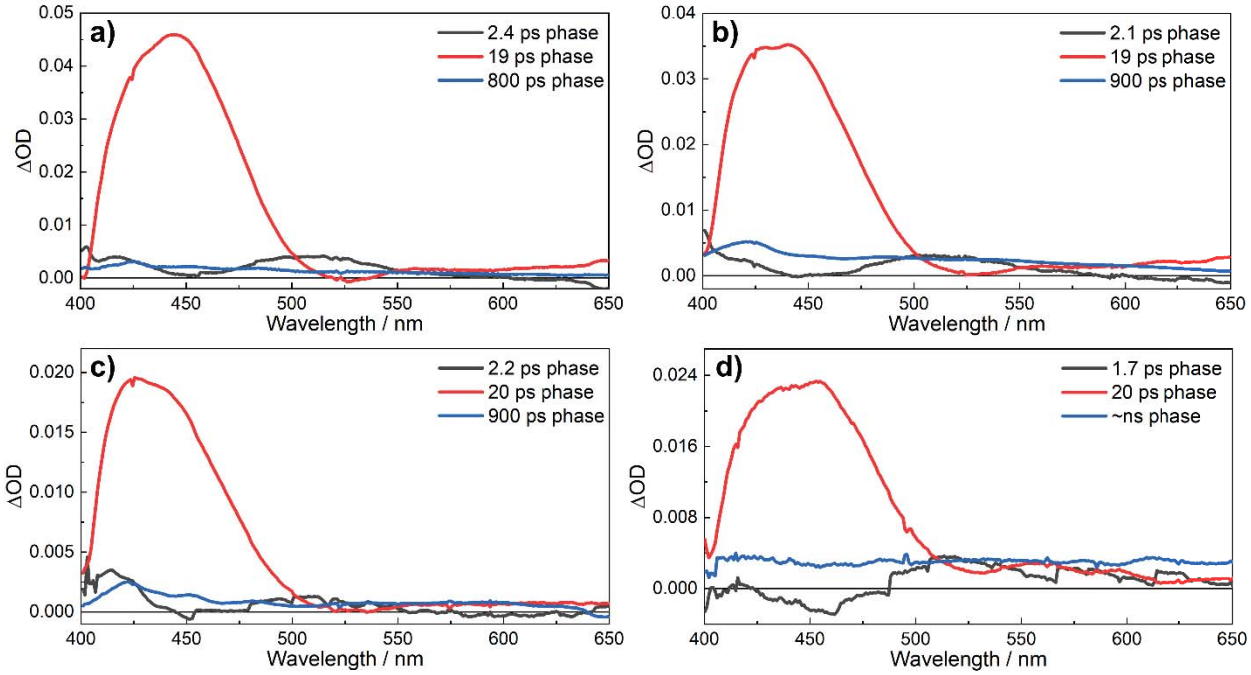

Fig. S16. DAS of isotropic transient absorption data of $FAD^{\bullet-}$ in GOX under excitation at 390 nm, with samples prepared by photoreduction in the presence of EDTA at pH 10.1 (a) and 2-ME (b) at pH 10.1, or through chemical reduction with $Na_2S_2O_4$ at pH 7.4 (c) and pH 13.0 (d).

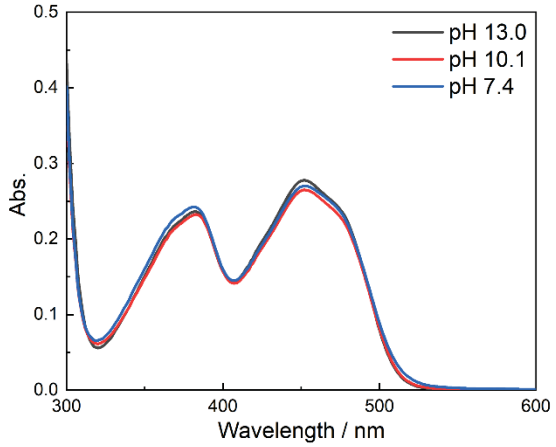

Fig. S17. Steady-state absorption spectra of the freshly prepared FAD_{ox} samples of GOX at different pH values.

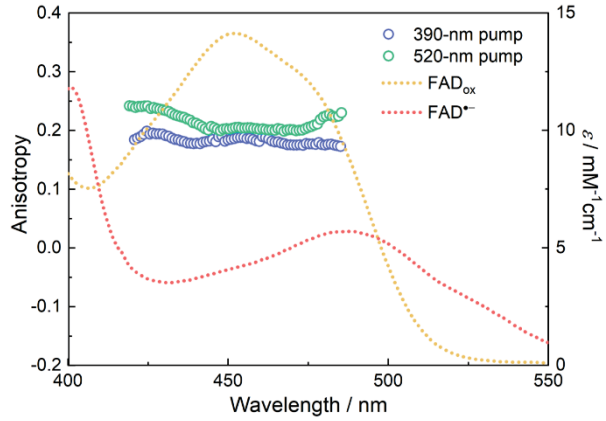

Fig. S18. Transient anisotropy in the induced absorption regions calculated based on polarized DAS of the ~20 ps phase under two excitation conditions in GOX (colored circles). The steady-state absorption spectra of FAD_{ox} and $FAD^{\bullet-}$ in GOX are also shown as references (dashed lines).

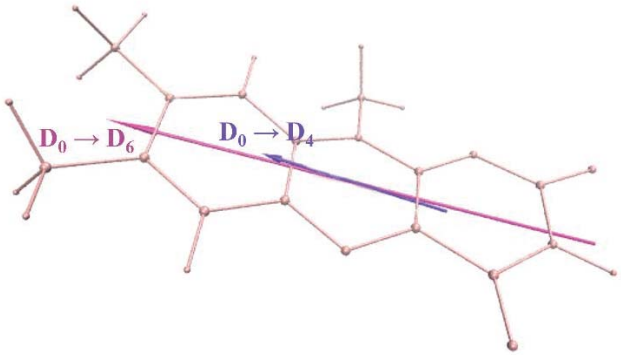

Fig. S19. Orientations of the transition dipole moments of the $D_0 \rightarrow D_4$ and $D_0 \rightarrow D_6$ transitions of an anionic flavin radical from TDDFT calculations.

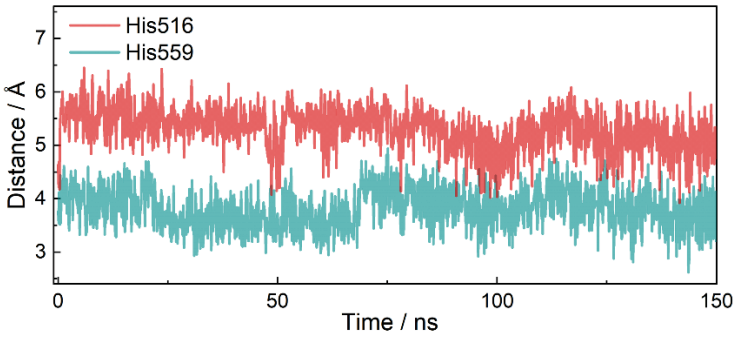

Fig. S20. The minimal ring-to-ring distance between $FAD^{\bullet-}$ and His516 or His559 in the MD simulation of GOX.

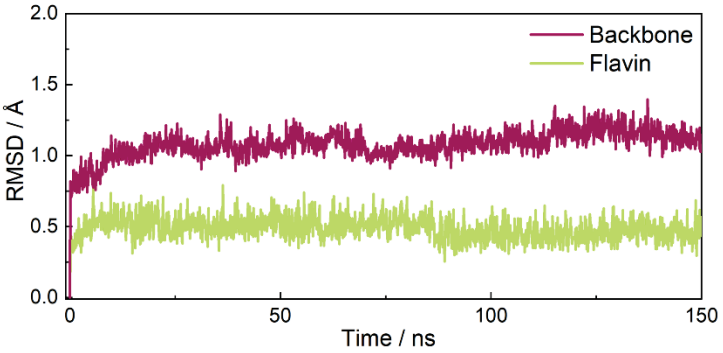

Fig. S21. RMSD for the backbone atoms of the protein and non-hydrogen atoms of $FAD^{\bullet-}$ in GOX in the 150 ns MD simulation.

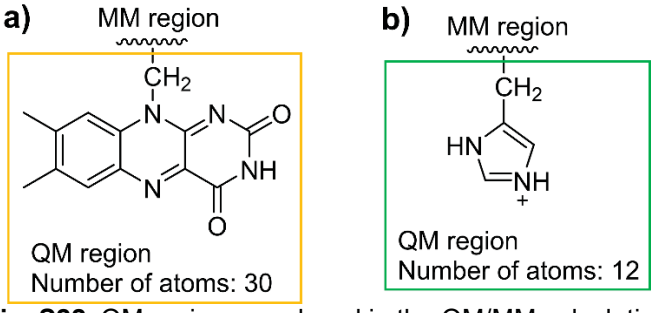

Fig. S22. QM regions employed in the QM/MM calculations of FAD (a) and His559 (b) in GOX.

Supplementary Tables

Table S1. Experimental conditions for preparing reduced flavin species in this study.

Species	Protein	Reductant (chemical reduction)	Hole scavenger (photoreduction)	pH
$FAD^{\bullet-}$	GOX	$Na_2S_2O_4$	-	7.6, 10.1, 13.0
$FAD^{\bullet-}$	GOX	-	EDTA	10.1
$FAD^{\bullet-}$	GOX	-	2-ME	10.1
$FADH^-$	GOX	D(+)-glucose	-	7.6
$FAD^{\bullet-}$	COX	$Na_2S_2O_4$	-	8.1
$FAD^{\bullet-}$	MSOX	$Na_2S_2O_4$	-	8.0, 8.5
$FAD^{\bullet-}$	DAAO	-	2-ME	8.1
$FMN^{\bullet-}$	NMO	P3N	-	8.0

Table S2. Parameters from the global multi-exponential fit for fluorescence decays of flavin species in GOX and COX. The pre-exponential factor of each component is given in parentheses following the time constants.

	τ_1 (ps)	τ_2 (ps)	τ_3 (ps)
FAD_{ox} (GOX)	1.1 (0.62)	4.3 (0.34)	120 (0.04)
$FADH^-$ (GOX)	800 (1.00)		
As-prepared (oxidized) COX	0.29 (0.91)	440 (0.09)	
Reduced COX	0.30 (0.90)	320 (0.10)	

Table S3. Time constants from the global fit of the transient absorption kinetics of anionic flavin radicals (520-nm excitation), as well as positively charged residues close (within 5 Å) to the flavins, in the five flavoprotein oxidases.

Protein	τ (ps)	Close-by positively charged residue
GOX	19	His559, His516
COX	10	His466, Arg89*
MSOX	15	Lys384, Arg49
DAAO	18	Arg283
NMO	21	His133

*For His99, see the main text.

Table S4. Molecular orbital energies of selected residue side chains in the one-electron reduced form. Energies were obtained on the geometry optimized at the ωB97X-D3/ma-def2-TZVP level in vacuum.

Residue	ϵ_{HOMO} (eV)
Arginine	−5.92
Asparagine	−0.14
Histidine (doubly protonated)	−5.24
Histidine (N_ε protonated)	−0.77
Histidine (N_δ protonated)	−0.42
Lysine	−3.77
Methionine	−0.28
Phenylalanine	−0.17
Tyrosine	−0.28
Tryptophan	−0.08

Table S5. pKa calculations based on MDFE simulations. Variables are defined in *Note 6*. Statistical uncertainty in parentheses estimated as twice the standard deviation of block averages, with each data set being divided into five blocks. N/A, not applicable.

	With $FAD^{\bullet-}$ (His516, GOX)	With $FADH^-$ (His516, GOX)	Explicit solvent (dipeptide)
ΔG (kcal/mol)	9.9 (0.9)	4.6 (0.5)	1.1 (0.2)
$\Delta\Delta G_{calc}$ (kcal/mol)	8.8 (0.9)	3.5 (0.5)	N/A
pK_a (calc.)	13.5 (0.7)	9.6 (0.4)	N/A
p$K_{a,}$ (exper.)	N/A	8.1*	7.0

*The experimental value is from Ref (42).

Table S6. CHELPG atomic charges of histidine in the neutral radical form. The CHARMM force field atom names are used. The calculations were performed at the ωB97X-D3/ma-def2-TZVP level.

Atom	CHELPG atomic charges
CB	-0.0797
HB1	0.0488
HB2	0.0499
CE1	-0.4904
HE1	0.2135
CD2	-0.2764
HD2	0.1751
ND1	-0.1780
HD1	0.2906
NE2	-0.1887
HE2	0.3081
CG	0.1271

Table S7. Energies in eq. s7 calculated for FAD_{ox}, $FAD^{\bullet-}$, $HisH_2^+$ and $HisH_2^{\bullet}$. Energies were computed at the PWPB95-D4/def2-QZVPP level with thermostatistical corrections at the ωB97X-D3/ma-def2-TZVP level, and given relative to FAD_{ox} and $HisH_2^+$, respectively; The solvation energies were calculated with the SMD solvation model at the M06-2X/6-31G* level. Geometries were optimized at the ωB97X-D3/ma-def2-TZVP level prior to energy calculations.

	G_g (kJ/mol)	ΔG_{solv} (kJ/mol)	ΔG_s (kJ/mol)
FAD_{ox}	0.0	−73.6	−367.3
$FAD^{\bullet-}$	−176.1	−250.7	
$HisH_2^+$	0.0	−242.4	−178.2
$HisH_2^{\bullet}$	−389.6	−16.9	

SI References

1. A. Hense, E. Herman, S. Oldemeyer, T. Kottke, Proton transfer to flavin stabilizes the signaling state of the blue light receptor plant cryptochrome. *J. Biol. Chem.* **290**, 1743–1751 (2015).
2. L. Nag, P. Sournia, H. Myllykallio, U. Liebl, M. H. Vos, Identification of the TyrOH•+ radical cation in the flavoenzyme TrmFO. *J. Am. Chem. Soc.* **139**, 11500–11505 (2017).
3. V. Massey, G. Palmer, On the existence of spectrally distinct classes of flavoprotein semiquinones. A new method for the quantitative production of flavoprotein semiquinones. *Biochemistry* **5**, 3181–3189 (1966).
4. D. Su, *et al.*, Fluorescence properties of flavin semiquinone radicals in nitronate monooxygenase. *ChemBioChem* **20**, 1646–1652 (2019).
5. S. P. Laptenok, P. Nuernberger, A. Lukacs, M. H. Vos, in *Methods in molecular biology, fluorescence spectroscopy and microscopy: methods and protocols,* (Humana, New York, 2014), vol. 1076, pp. 321–336.
6. B. Zhuang, D. Seo, A. Aleksandrov, M. H. Vos, Characterization of light-induced, short-lived interacting radicals in the active site of flavoprotein ferredoxin-NADP+ oxidoreductase. *J. Am. Chem. Soc.* **143**, 2757–2768 (2021).
7. J. J. Snellenburg, S. P. Laptenok, R. Seger, K. M. Mullen, I. H. M. van Stokkum, Glotaran: a Java-based graphical user interface for the R package TIMP. *J. Stat. Softw.* **49** (2012).
8. Y. S. Lin, G. De Li, S. P. Mao, J. Da Chai, Long-range corrected hybrid density functionals with improved dispersion corrections. *J. Chem. Theory Comput.* **9**, 263–272 (2013).
9. J. Zheng, X. Xu, D. G. Truhlar, Minimally augmented Karlsruhe basis sets. *Theor. Chem. Acc.* **128**, 295–305 (2011).
10. H. Neugebauer, F. Bohle, M. Bursch, A. Hansen, S. Grimme, Benchmark study of electrochemical redox potentials calculated with semiempirical and DFT methods. *J. Phys. Chem. A* **124**, 7166–7176 (2020).
11. A. V. Marenich, C. J. Cramer, D. G. Truhlar, Universal solvation model based on solute electron density and on a continuum model of the solvent defined by the bulk dielectric constant and atomic surface tensions. *J. Phys. Chem. B* **113**, 6378–6396 (2009).
12. R. F. Ribeiro, A. V. Marenich, C. J. Cramer, D. G. Truhlar, Use of solution-phase vibrational frequencies in continuum models for the free energy of solvation. *J. Phys. Chem. B* **115**, 14556–14562 (2011).
13. F. Neese, The ORCA program system. *Wiley Interdiscip. Rev. Comput. Mol. Sci.* **2**, 73–78 (2012).
14. J. C. Phillips, *et al.*, Scalable molecular dynamics with NAMD. *J. Comput. Chem.* **26**, 1781–1802 (2005).
15. J. Huang, *et al.*, CHARMM36m: an improved force field for folded and intrinsically disordered proteins. *Nat. Methods 2016 141* **14**, 71–73 (2016).
16. W. L. Jorgensen, J. Chandrasekhar, J. D. Madura, R. W. Impey, M. L. Klein, Comparison of simple potential functions for simulating liquid water. *J. Chem. Phys.* **79**, 926–935 (1983).
17. A. Aleksandrov, A molecular mechanics model for flavins. *J. Comp. Chem.* **40**, 2834–2842 (2019).
18. M. H. M. Olsson, C. R. SØndergaard, M. Rostkowski, J. H. Jensen, PROPKA3: Consistent treatment of internal and surface residues in empirical p K a predictions. *J. Chem. Theory Comput.* **7**, 525–537 (2011).
19. T. Simonson, J. Carlsson, D. A. Case, Proton binding to proteins: pKa calculations with explicit and implicit solvent models. *J. Am. Chem. Soc.* **126**, 4167–4180 (2004).
20. T. Darden, D. York, L. Pedersen, Particle mesh Ewald: An N·log(N) method for Ewald sums in large systems. *J. Chem. Phys.* **98**, 10089–10092 (1993).
21. H. J. C. Berendsen, J. P. M. Postma, W. F. van Gunsteren, A. DiNola, J. R. Haak, Molecular dynamics with coupling to an external bath. *J. Chem. Phys.* **81**, 3684 (1998).
22. M. J. Field, The pDynamo program for molecular simulations using hybrid quantum chemical and molecular mechanical potentials. *J. Chem. Theory Comput.* **4**, 1151–1161 (2008).
23. C. M. Breneman, K. B. Wiberg, Determining atom-centered monopoles from molecular electrostatic potentials. The need for high sampling density in formamide conformational

analysis. *J. Comput. Chem.* **11**, 361–373 (1990).
24. L. Zanetti-Polzi, M. Aschi, A. Amadei, I. Daidone, Alternative electron-transfer channels ensure ultrafast deactivation of light-induced excited states in riboflavin binding protein. *J. Phys. Chem. Lett.* **8**, 3321–3327 (2017)
25. A. D. Becke, A new mixing of Hartree-Fock and local density-functional theories. *J. Chem. Phys.* **98**, 1372–1377 (1993).
26. M. M. Francl, *et al.*, Self-consistent molecular orbital methods. XXIII. A polarization-type basis set for second-row elements. *J. Chem. Phys.* **77**, 3654 (1998).
27. B. R. Brooks, *et al.*, CHARMM: A program for macromolecular energy, minimization, and dynamics calculations. *J. Comput. Chem.* **4**, 187–217 (1983).
28. S. C. Harvey, Treatment of electrostatic effects in macromolecular modeling. *Proteins Struct. Funct. Bioinforma.* **5**, 78–92 (1989).
29. V. Massey, M. Stankovich, P. Hemmerich, Light-mediated reduction of flavoproteins with flavins as catalysts. *Biochemistry* **17**, 1–8 (1978).
30. R. Traber, H. E. A. Kramer, P. Hemmerich, Mechanism of light-induced reduction of biological redox centers by amino acids. a flash photolysis study of flavin photoreduction by ethylenediaminetetraacetate and nitrilotriacetate. *Biochemistry*. **21**, 1687–1693 (1982).
31. N. Nunthaboot, *et al.*, Simultaneous analysis of ultrafast fluorescence decays of FMN binding protein and its mutated proteins by molecular dynamic simulation and electron transfer theory. *J. Phys. Chem. B* **112**, 13121–13127 (2008).
32. L. Nag, A. Lukacs, M. H. Vos, Short-lived radical intermediates in the photochemistry of glucose oxidase. *ChemPhysChem* **20**, 1793–1798 (2019).
33. D. Su, C. Smitherman, G. Gadda, A metastable photoinduced protein–flavin adduct in choline oxidase, an enzyme not involved in light-dependent processes. *J. Phys. Chem. B* **124**, 3936–3943 (2020).
34. M. Enescu, L. Lindqvist, B. Soep, Excited-state dynamics of fully reduced flavins and flavoenzymes studied at subpicosecond time resolution. *Photochem. Photobiol.* **68**, 150–156 (1998).
35. F. Lacombat, P. Plaza, M. A. Plamont, A. Espagne, Photoinduced chromophore hydration in the fluorescent protein Dreiklang is triggered by ultrafast excited-state proton transfer coupled to a low-frequency vibration. *J. Phys. Chem. Lett.* **8**, 1489–1495 (2017).
36. P. Müller, K. Brettel, [Ru(bpy)3]2+ as a reference in transient absorption spectroscopy: Differential absorption coefficients for formation of the long-lived 3MLCT excited state. *Photochem. Photobiol. Sci.* **11**, 632–636 (2012).
37. W. W. Parson, *Modern optical spectroscopy: with exercises and examples from biophysics and biochemistry,* (Springer, Berlin, ed. 2, 2015).
38. A. Warshel, F. Sussman, G. King, Free energy of charges in solvated proteins: microscopic calculations using a reversible charging process. *Biochemistry* **25**, 8368–8372 (2002).
39. T. Simonson, Free energy calculations: Approximate methods for biological macromolecules. *Springer Ser. Chem. Phys.* **86**, 423–461 (2007).
40. A. Aleksandrov, T. Simonson, Molecular dynamics simulations of the 30S ribosomal subunit reveal a preferred tetracycline binding site. *J. Am. Chem. Soc.* **130**, 1114–1115 (2008).
41. A. Aleksandrov, J. Proft, W. Hinrichs, T. Simonson, Protonation patterns in tetracycline:Tet repressor recognition: simulations and experiments. *ChemBioChem* **8**, 675–685 (2007).
42. J. P. Roth, J. P. Klinman, Catalysis of electron transfer during activation of O2 by the flavoprotein glucose oxidase. *Proc. Natl. Acad. Sci. U. S. A*. **100**, 62–67 (2003).
43. M. Namazian, M. L. Coote, Accurate calculation of absolute one-electron redox potentials of some para-quinone derivatives in acetonitrile. *J. Phys. Chem. A*. **111**, 7227–7232 (2007).
44. H. Ishikita, E. W. Knapp, Redox potential of quinones in both electron transfer branches of photosystem I. *J. Biol. Chem.* **278**, 52002–52011 (2003).
45. Y.-T. Kao, *et al.*, Ultrafast dynamics and anionic active states of the flavin cofactor in cryptochrome and photolyase. *J. Am. Chem. Soc*. **130**, 7695–7701 (2008).